Published in Topics in Fracture and Fatigue (ed. A. S. Argon), Springer Verlag, 1992, Chapter 1, pp. 1-58.

1

Peierls Framework for Dislocation Nucleation from a Crack Tip

J. R. Rice, G. E. Beltz, and Y. Sun

ABSTRACT Dislocation nucleation from a stressed crack tip is analyzed based on the Peierls concept, in which a periodic relation between shear stress and atomic shear displacement is assumed to hold along a slip plane emanating from a crack tip. This approach allows some small slip displacement to occur near the tip in response to small applied loading and, with increase in loading, the incipient dislocation configuration becomes unstable and leads to a fully formed dislocation which is driven away from the crack. An exact solution for the loading at that nucleation instability was developed using the J-integral for the case when the crack and slip planes coincide (Rice, 1992). Solutions are discussed here for cases when they do not. The results were initially derived for isotropic materials and some generalizations to take into account anisotropic elasticity are noted here. Solutions are also given for emission of dissociated dislocations, especially partial dislocation pairs in fcc crystals. The level of applied stress intensity factors required for dislocation nucleation is shown to be proportional to $\sqrt{\gamma_{us}}$ where γ_{us}, the *unstable stacking* energy, is a new solid state parameter identified by the analysis. It is the maximum energy encountered in the block-like sliding along a slip plane, in the Burgers vector direction, of one half of a crystal relative to the other. Approximate estimates of γ_{us} are summarized, and the results are used to evaluate brittle versus ductile response in fcc and bcc metals in terms of the competition between dislocation nucleation and Griffith cleavage at a crack tip. The analysis also reveals features of the near-tip slip distribution corresponding to the saddle point energy configuration for cracks that are loaded below the nucleation threshold, and some implications for thermal activation are summarized. Additionally, the analysis of dislocation nucleation is discussed in connection with the emission from cracks along bimaterial interfaces, in order to understand recent experiments on copper bicrystals and copper/sapphire interfaces, and we discuss the coupled effects of tension and shear stresses along slip planes at a crack tip, leading to shear softening and eased nucleation.

Reprinted from the book, *Topics in Fracture and Fatigue* edited by A.S. Argon, 1992

1.1 Introduction

Armstrong (1966) and Kelly et al. (1967) advanced the viewpoint of brittle versus ductile response as the competition between Griffith cleavage and plastic shear at a crack tip. The latter proposed that the response of a crystal or grain boundary should be treated by comparing the ratio of the largest tensile stress to the largest shear stress close to a crack tip with the ratio of the ideal cleavage stress to the ideal shear stress. Armstrong compared the applied stress necessary to meet the Griffith condition with the stress to shear apart a dislocation dipole near a crack tip, and thereby noted the importance of the dimensionless combination $\gamma_s/\mu b$ (γ_s = surface energy, μ = shear modulus, b = magnitude of the Burgers vector) as an index of how relatively easy it was for the shear process to occur before cleavage. Subsequently Rice and Thomson (1974) specifically modeled the shear process as the nucleation of a dislocation from a stressed crack tip. The Rice and Thomson approach made use of elasticity solutions for a fully formed dislocation (i.e., a dislocation with slip equal to the Burgers vector $\boldsymbol{b}$ of some complete or partial lattice dislocation) and a core cut-off parameter had to be introduced to derive a nucleation criterion. Their analysis showed, likewise, the importance of large $\gamma_s/\mu b$ and also of low core energy (large r_c/b, where r_c is the core cut-off radius in their analysis) for ductile response.

Recent treatments of the Rice-Thomson model have evolved to characterizing the crack-tip competition in terms of the parameters G_{cleave}, the energy release rate for cleavage and G_{disl}, the energy release rate associated with the emission of a single dislocation on a slip plane emanating from the crack tip. In its original form, the Rice-Thomson model treated dislocation emission by considering the stability of a straight dislocation line or a semicircular dislocation loop; both proceeded by assuming the existence of a freshly generated dislocation at a relatively small distance (turning out to be less than a few atomic spacings) away from the crack tip, on a slip plane which intersects the crack front. A drawback to this procedure, as well as the Peierls-type model to be discussed shortly, is that the analysis may be straightforwardly applied only to cases in which the slip plane(s) intersect the crack front. Following Mason (1979), however, we may envision a scenario in which dislocations are emitted when a moving crack front undergoes local deviations which bring it into line with a potentially active slip plane. Another drawback to the Rice-Thomson treatment is that it involves the core cutoff radius, an uncertain parameter. Here, following a suggestion by Argon (1987), the Peierls (1940) concept is used in an analysis of dislocation formation at a crack tip. That is, a periodic relation is assumed to hold between shear stress and sliding displacement along a crystal slip plane emanating from a crack tip, and a solution is then derived for the critical external loading which corresponds to dislocation nucleation.

A first report on this approach has been given by Rice (1992). We follow the text and format of that work closely here, adopting entire sections where appropriate. We also enlarge on the development to review exact numerical solutions, anisotropic effects, coupled shear and tension, thermal activation, and bimaterial interface cracks.

With the results derived in the Peierls framework, we shall have no further need for introduction of the poorly defined core cut-off at a crack tip in analyzing nucleation phenomena. Indeed, the results show that no feature resembling a fully formed dislocation is present at the crack tip prior to the instability. The instability begins a slip event leading to a fully formed dislocation which moves away from the crack tip. Prior to the instability there exists only an incipient dislocation in the form of a nonlinear shear distribution along a slip plane, with maximum deformation equivalent to a slip at the crack tip of generally less than a half of that of the fully formed dislocation. This agrees with the suggestion by Argon (1987) that nucleation instability should occur at a slip less than that of the dislocation which ultimately emerges. The Peierls concept has also been used in a recent analysis of dislocation nucleation by Schoeck (1991). His analysis was somewhat more approximate and did not uncover the exact solution for nucleation within the Peierls framework that is derived here. The results by Rice (1992) identified a new solid state parameter, denoted γ_{us} and called the *unstable stacking* energy, which characterizes the resistance to dislocation nucleation.

1.2 Description of Model

Suppose that a crack tip intersects one of the possible slip planes in a ductile crystal (Fig. 1.1(a)). The question addressed is that of what loading of the cracked solid suffices to nucleate a dislocation from the tip, assuming that cleavage decohesion does not occur first. By adopting the Peierls (1940) concept, the shear stress τ along the slip plane is regarded as a (periodic) function of the slip displacement δ along it. Thus, the problem addressed consists of an externally loaded solid containing a crack with traction-free surfaces, and with the additional boundary condition that the shear traction τ must be a function of the slip displacement δ along a plane of displacement discontinuity emanating from the crack tip. For the present we assume that there is a discontinuity of slip displacement only along that plane. More precise models in which there are discontinuities in both shear and opening displacement (the latter relating to dilatancy of an atomic array during large shear and, also, to the presence of tensile stress σ across the slip plane) are discussed by Beltz and Rice (1991, 1992a) and Sun et al. (1992). Hence, if $\boldsymbol{s}$ and $\boldsymbol{n}$ are unit vectors in the slip direction and normal to the slip plane, then $\delta = u_s^+ - u_s^-$ where $u_s = \boldsymbol{s} \cdot \boldsymbol{u}$; $\boldsymbol{u}$ is the displacement vector and $+, -$ refer to the two sides of the slip plane with $\boldsymbol{n}$ pointing

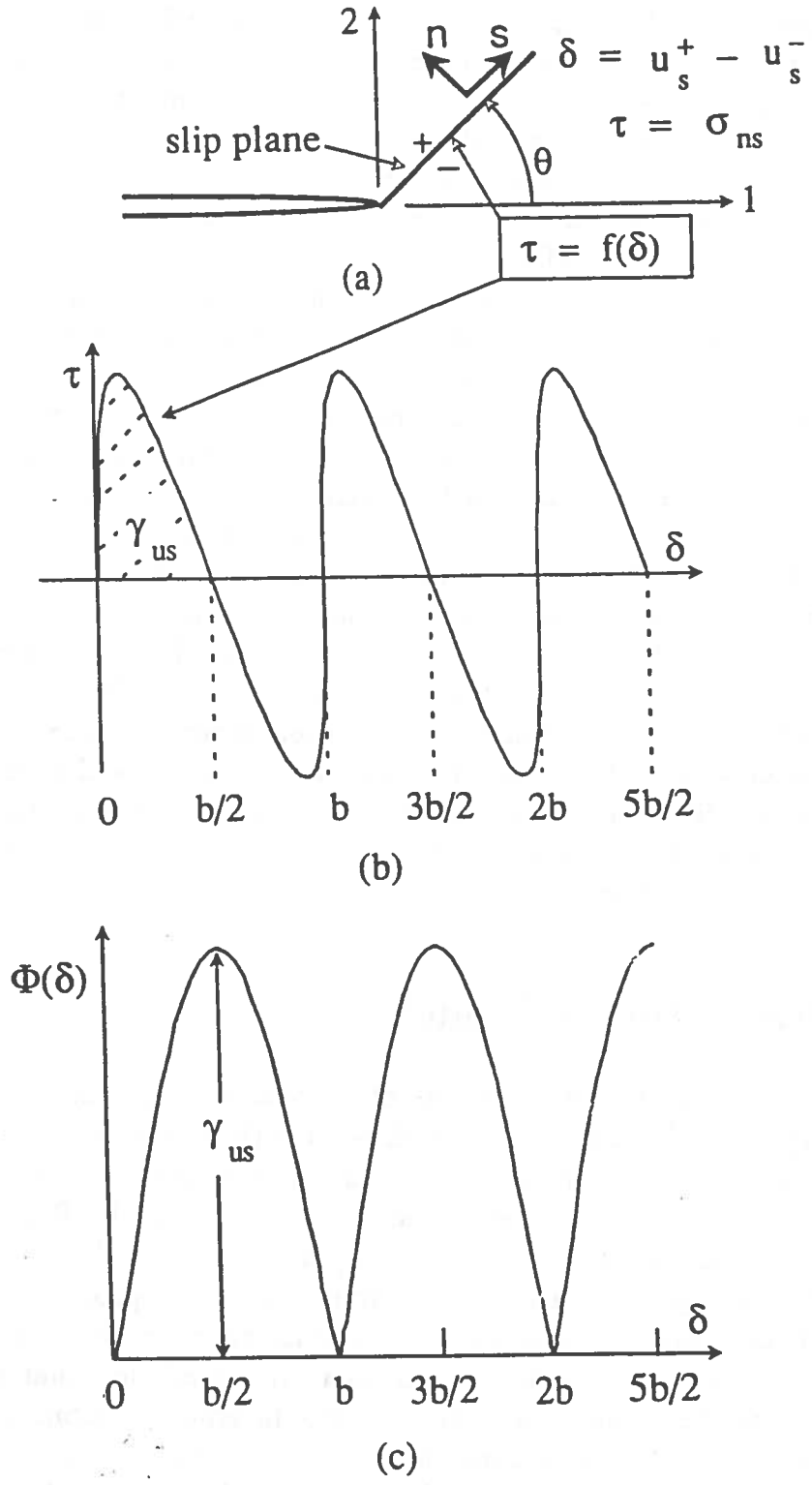

FIGURE 1.1. (a) Crystal slip plane emanating from crack tip. (b) Periodic relation between stress and shear displacement discontinuity (see discussion in connection with next figure to understand basis for vertical tangent at zero slip). (c) Energy associated with slip discontinuity.

from $-$ to $+$. Within the present simplification, other components of $\boldsymbol{u}$ are continuous. Also, $\tau = n_\alpha \sigma_{\alpha\beta} s_\beta = \sigma_{ns}$ where $\sigma_{\alpha\beta}$ is the stress tensor.

The τ *vs.* δ relation is assumed to have a form like in Fig. 1.1(b), i.e., a periodic function with period b equal to the Burgers vector of a full dislocation, and with an axis crossing in-between, at $b/2$ in lattices with simple symmetry. Ways of estimating the form of the relation, and why it has been drawn with a vertical tangent at $\delta = 0$ and b, are discussed below; adaptations of concepts so as to deal with complex dislocations having stacking faults or anti-phase boundaries are discussed in a later section. Weertman (1981) analyzed a similar model but with the τ *vs.* δ relation in the form of a rectangular wave.

The result derived by Rice (1992), exactly for a special geometry and approximately in all cases, is that dislocation nucleation occurs under critical crack tip stress intensity factors which scale with $\sqrt{\gamma_{\rm us}}$. Here $\gamma_{\rm us}$, the unstable stacking energy, is identified in Fig. 1.1(b) as the area under the τ *vs.* δ curve between $\delta = 0$ and $\delta = b/2$ (more generally, $\gamma_{\rm us}$ is the area between $\delta = 0$ and the first δ at which $\tau = 0$ again). Figure 1.1(c) shows the energy per unit area of the slip plane, $\Phi = \int \tau d\delta$. Thus $\gamma_{\rm us}$ is the maximum value of Φ. We may take the viewpoint that the same τ *vs.* δ relation could be used to describe the block-like shear, along a slip plane, of one half of a perfect lattice relative to the other. Hence Φ (or, more accurately, a related energy Ψ introduced below) corresponds to the γ-energy plot of Vitek (1968) and Vitek et al. (1972) and $\gamma_{\rm us}$, the maximum value of Φ (and of Ψ) along the slip path, is the energy barrier to be overcome in block-like shear.

To understand the τ *vs.* δ relation, consider the states of shear of an initially rectangular lattice illustrated in Fig. 1.2. The relative shear displacement of the central pair of planes is denoted Δ; these are separated by distance h and are the pair of planes which will ultimately be displaced a lattice distance b. Lattice configurations (a) to (d), starting at the lower left and going clockwise, correspond to point (a) to (d) on the τ versus Δ curve. All the configurations shown are homogeneous in the direction of the shear displacement, but not perpendicular to it. When sufficiently sheared, like in (c) and (d), there exist configurations in which the lattice is not homogeneously strained, like it is in (b), but rather for which the central pair of planes corresponds to a Δ along the descending part of the τ versus Δ relation, while the crystal outside is stressed at the same level at an amount of shear corresponding to the rising part of the curve. Position (d) corresponds to the unstressed but unstable equilibrium state for which the central pair of lattice planes are displaced by $b/2$ while the crystal outside is unstrained. This is the unstable stacking configuration and the work to create it (area under τ versus Δ between $\Delta = 0$ and $b/2$) is $\gamma_{\rm us}$, the same $\gamma_{\rm us}$ of Figs. 1.1(b) and (c), as explained next.

Although the configurations considered in Fig. 1.2 are homogeneous in the direction of shear, we follow Peierls (1940) in applying the τ versus Δ

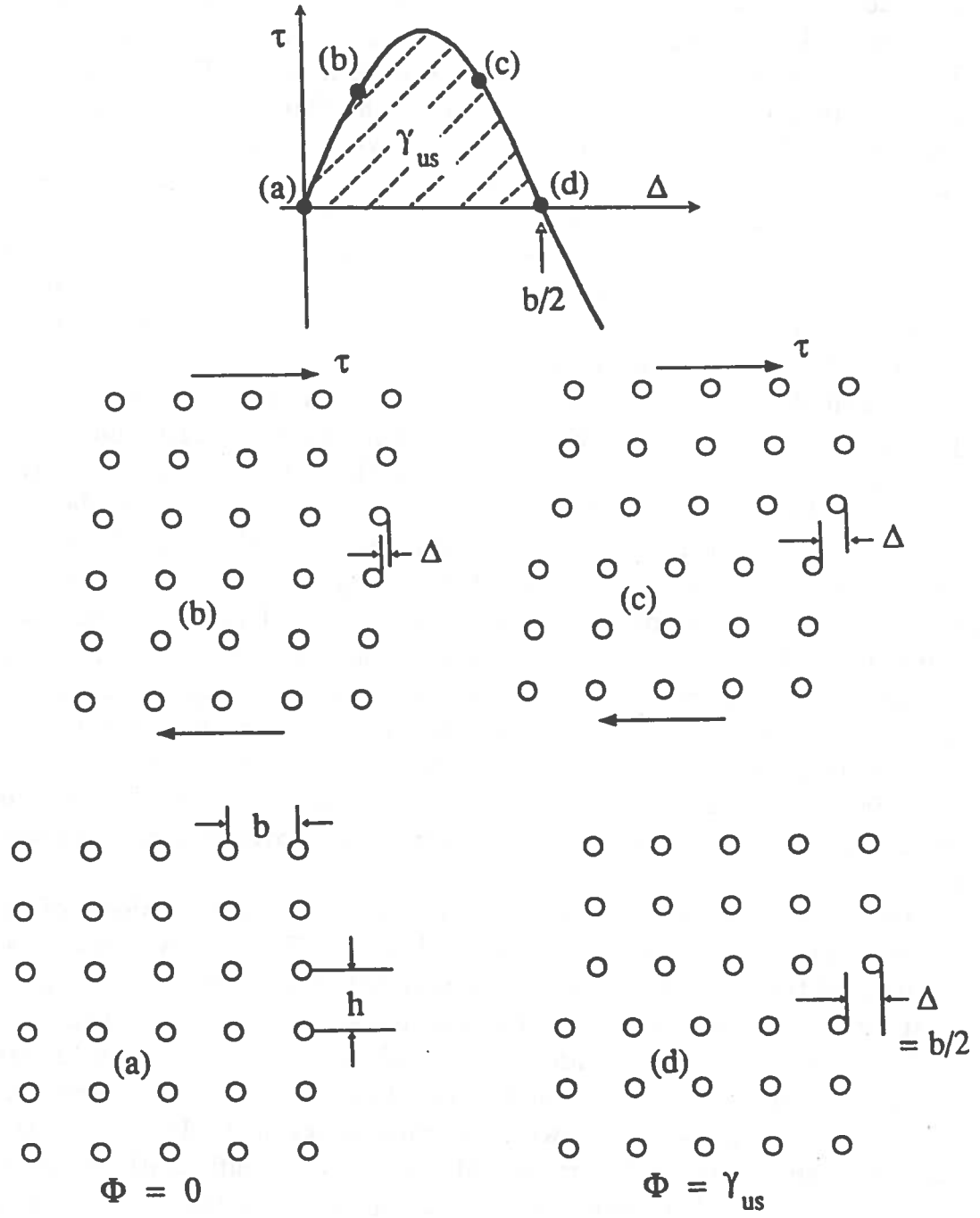

FIGURE 1.2. Various states of shear for a simple cubic lattice; state (d) shows the unstable stacking configuration, with energy γ_{us} per unit area of slip plane.

relation locally to states of inhomogeneous shear like along the slip plane in Fig. 1.1(a). Since that inhomogeneous shear is modeled here as a displacement discontinuity, of amount δ, along a cut of zero thickness in an elastic continuum, it is sensible to identify δ not with Δ, which denotes relative displacement of points a distance h apart, but rather to write $\Delta = \delta + h\tau/\mu$ so that relative displacement Δ of atomic planes at spacing h is composed of the discontinuity δ on the mathematical cut plus an additional amount due to elastic shearing by amount τ/μ over a distance h perpendicular to the cut; μ is the shear modulus. Thus, if $\tau = F(\Delta)$, of period b, describes the τ versus Δ relation of Fig. 1.2, where $F(0) = 0$ and $\mu = hF'(0)$, then the τ versus δ relation, $\tau = f(\delta)$, is given parametrically by $\tau = F(\Delta)$ and $\delta = \Delta - h\tau/\mu = \Delta - F(\Delta)/F'(0)$. This means that the resulting $\tau = f(\delta)$ is of period b and that $f'(\delta)$ is unbounded at $\delta = 0$, as illustrated in Fig. 1.1(b). The transformation from Δ to δ as displacement variable preserves the area, namely γ_{us}, under the τ *vs.* displacement curve between the origin and the next zero of τ. An energy $\Psi(\Delta)$ may be defined from $\tau d\Delta = d\Psi$; it is the form in which an energy of sheared configurations has been calculated from atomic models (e.g., Vitek, 1968; Vitek et al., 1972; Yamaguchi et al., 1981; Sun et al., 1991). Given that the energy $\Phi(\delta)$ of Fig. 1.1(c) satisfies $\tau d\delta = d\Phi$, the relation $\delta = \Delta - h\tau/\mu$ shows that $d\Phi = d\Psi - h\tau d\tau/\mu$ and thus that $\Phi(\delta) = \Psi(\Delta) - h\tau^2(\Delta)/2\mu$.

The simplest case of a $\tau = F(\Delta)$ relation is the Frenkel sinusoidal function

$$\tau = (\mu b/2\pi h)\sin(2\pi\Delta/b), \tag{1.1}$$

in which case,

$$\delta = \Delta - (b/2\pi)\sin(2\pi\Delta/b) \tag{1.2}$$

and the energies Ψ and Φ are

$$\Psi = (\mu b^2/2\pi^2 h)\sin^2(\pi\Delta/b), \text{ and } \Phi = (\mu b^2/2\pi^2 h)\sin^4(\pi\Delta/b). \tag{1.3}$$

In this case γ_{us}, which is the common maximum of Φ and Ψ, is given by $\gamma_{us} = \mu b^2/2\pi^2 h$, an estimate that will be considered subsequently along with others. The plots in Figs. 1.1(b), 1.1(c) and 1.2 have been drawn based on the Frenkel sinusoid.

1.3 Analysis of Simplified Geometry with Coincident Crack and Slip Planes

This section repeats the major result of Rice (1992). While geometries like in Fig. 1.1(a), typically loaded by tensile, or predominantly tensile, forces relative to the crack plane are of primary interest, the problem posed there

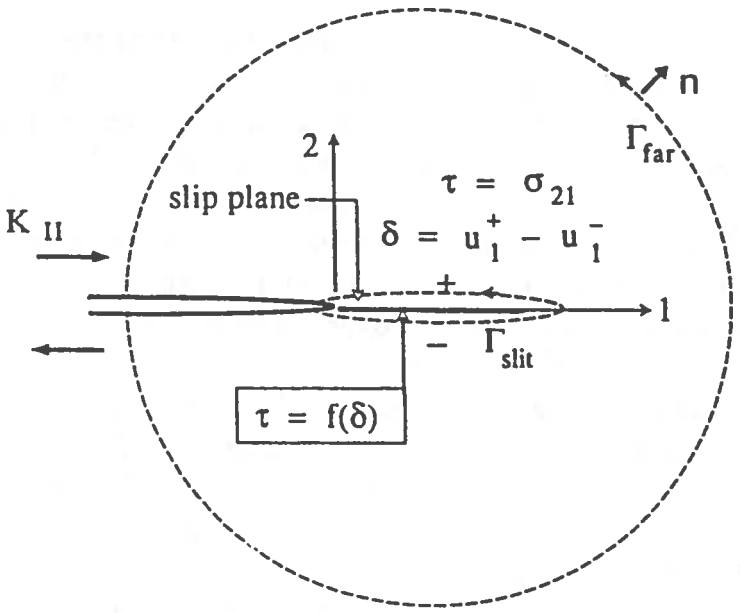

FIGURE 1.3. Coincident crack and slip plane, mode II loading.

is solvable only by numerical methods (Beltz and Rice, 1991a,b). Tensile loading of that configuration of Fig. 1.1(a) causes high shear stress τ (at least, when slip δ is precluded) along any slip plane in the general range of, say, $\theta = 30°$ to $120°$; the mode I crack tip field has highest shear stress along $\theta \approx 70°$. Some of the same features of the configuration of Fig. 1.1(a), namely, shear along a highly stressed plane emanating from the crack tip, are preserved in the simplified configuration of Fig. 1.3, for which an exact solution will be derived. In that simplified case, the most stressed slip plane is assumed to be coplanar with the crack ($\theta = 0$), with $\boldsymbol{s}$ in the x_1 direction, so emerging dislocations are of edge character relative to the tip, and the external loading is by in-plane (mode II) shear. A nearly identical analysis may be followed when $\boldsymbol{s}$ is in the x_3 direction, so that emerging dislocations are of screw type relative to the tip, and loading is by anti-plane shear (mode III).

Along the prolongation of the crack into the slip plane in Fig. 1.3, we have $\delta = u_1^+ - u_1^-$ and $\tau = \sigma_{21}$, where $\tau = f(\delta)$ like in Fig. 1.1(b); u_2 and u_3 are continuous there. Recognizing that this configuration is being analyzed as a simplified analog of more realistic tensile-loaded cases like in Fig. 1.1(a), we do not extend applicability of the τ versus δ relation back onto the crack faces in Fig. 1.3 but, rather, assume that the crack faces are traction free ($\sigma_{2j} = 0, j = 1, 2, 3$).

The crack is assumed to be sufficiently long that any region near its tip where significant slip develops, prior to unstable dislocation nucleation, is assumed to be of negligible length compared to crack length and other overall dimensions of the cracked solid, such as distance to boundaries and to points of external force application. In that case it suffices to consider the

crack as a semi-infinite slit in an unbounded solid, with all loadings applied at infinitely remote distance so that all we need consider is the singular crack tip stress field, characterized by stress intensity factors, $K_{\rm I}, K_{\rm II}, K_{\rm III}$, that the loadings would induce in the linear elastic model of the actual solid. At present, only $K_{\rm II}$ is assumed to be non zero, such that the stress field ahead of the crack tip ($x_2 = 0, x_1 > 0$) in the linear elastic model of our solid, when restrained against slip δ, is $\sigma_{21} \equiv \tau_0 = K_{\rm II}/\sqrt{2\pi r}, \sigma_{22} = \sigma_{23} = 0$, with $r = x_1$, and the Irwin energy release rate G is, in the isotropic case,

$$G = (1-\nu)K_{\rm II}^2/2\mu \tag{1.4}$$

where μ is the shear modulus and ν the Poisson ratio.

We now follow a similar argument to that used by Rice (1968 a,b), based on the path-independent J integral, in proof of the equivalence of the Griffith criterion $G = 2\gamma_s$ (γ_s = surface energy) for tensile crack growth under mode I loading to the criterion derived from the tensile-decohesion analog of the model described so far here (i.e., from a model in which σ_{22} is a function of opening displacement, $u_2^+ - u_2^-$, along the prolongation of the crack plane, with that function increasing to a maximum and then diminishing to zero at large opening displacements, such that its integral from 0 to ∞ is $2\gamma_s$). That same equivalence was demonstrated earlier by Willis (1967), using integral representations of the linear elastic solution for the field outside the decohesion zone, and the Willis method was also adapted by Rice (1992) to the present analysis of shear dislocation emission at a crack tip. See Eshelby (1970), Rice (1987), and Rice and Wang (1989) for related discussions.

The J integral is

$$J = \int_\Gamma [n_1 W(\nabla \boldsymbol{u}) - n_\alpha \sigma_{\alpha\beta} \partial u_\beta/\partial x_1]\, ds \tag{1.5}$$

where W is the strain energy density, $\sigma_{\alpha\beta} = \partial(W(\Delta \boldsymbol{u}))/\partial(\partial u_\beta/\partial x_\alpha)$ is the stress tensor, s is arc length, and, here, $\boldsymbol{n}$ is the unit outward normal to the path Γ, where Γ starts on the lower crack surface, surrounds the crack tip and any slip zone in its vicinity, and ends on the upper crack surface. The integral is independent of path when evaluated for any 2D solution $\boldsymbol{u}(\boldsymbol{x})$ of the elastostatic equilibrium equations $\partial\sigma_{\alpha\beta}/\partial x_\alpha = 0$, at least when the elastic properties are invariant to translation in the x_1 direction. The path independence applies not only for conventional stable elastic solutions corresponding to a minimum of the energy functional $U[\boldsymbol{u}(\boldsymbol{x})]$, but also to 2D fields $\boldsymbol{u}(\boldsymbol{x})$ corresponding to other extremals of $U[\boldsymbol{u}(\boldsymbol{x})]$ such as saddle-point configurations, of interest for activation over energy barriers; the field equations $\partial\sigma_{\alpha\beta}/\partial x_\alpha = 0$ are satisfied at all extrema. Here U is the energy of the stressed solid per unit distance along the crack front.

Since J has the same value for all paths which do not traverse the crack or slip zone ahead of it, we can advantageously evaluate J on two contours,

Γ_{far} and Γ_{slit}; Γ_{far} lies far from the crack tip and the nonlinear perturbation of the linear elastic field due to the incipient slip process near the tip, whereas Γ_{slit} coincides with the upper and lower surfaces of the slit lying ahead of the crack tip on which the displacement u_1 is discontinuous by (variable) amount δ. The value of J on Γ_{far} will depend only on the remote linear elastic field characterized by K_{II} and, as is well known in that case, the result is $J = G$. The value along Γ_{slit} can be written as

$$\begin{aligned} J &= -\int_0^\infty \sigma_{21}\partial(u_1^+ - u_1^-)/\partial x_1 dx_1 = -\int_0^\infty \tau \partial\delta/\partial x_1 dx_1 \\ &= \int_0^{\delta_{tip}} \tau d\delta \equiv \Phi(\delta_{tip}) \end{aligned} \tag{1.6}$$

where δ_{tip} is the slip displacement discontinuity at the crack tip. Since J is independent of path, the two evaluations must agree and hence the amount of slip at the crack tip associated with any static solution must satisfy

$$G \equiv (1-\nu)K_{II}^2/2\mu = \Phi(\delta_{tip}). \tag{1.7}$$

For anisotropic solids the same result applies but with $(1-\nu)/2\mu$ replaced with the appropriate compliance factor from the Stroh (1958) and Barnett and Asaro (1972) results relating G to K_{II}.

Thus as the applied K_{II} and hence G increases from zero, one first follows the rising branch of the $\Phi(\delta)$ function of Fig. 1.4, having solutions for δ_{tip} like that illustrated at point A. Such values of δ_{tip} [$= \delta(r)$ at $r = 0$] are reasonably assumed to correspond to functions $\delta(r)$ that give minima of $U[\delta(r)]$ and that represent an incipient, but not yet fully formed, dislocation at the crack tip. It is evident that no static solution can exist when G exceeds γ_{us}, the maximum value of Φ, and hence the incipient dislocation configuration discussed loses stability at

$$G \equiv (1-\nu)K_{II}^2/2\mu = \gamma_{us}, \tag{1.8}$$

which therefore corresponds to nucleation of a full dislocation. The slip δ_{tip} at the crack tip when instability is reached is well short of that (namely, b) for a full dislocation, and corresponds to $b/2$ in lattices with simple symmetry. Thus no feature resembling a fully formed dislocation is actually present at the crack tip prior to the instability at which the full dislocation is nucleated.

As further shown in Fig. 1.4, the equation $G = \Phi(\delta_{tip})$ for $G < \gamma_{us}$ has multiple roots, illustrated by solution points A, C, A', A'', ... Points A', A'', etc. have a clear interpretation as corresponding to incipient dislocation configurations after one, two, etc. full dislocations have already been formed from the crack tip. Since A and A' may be presumed to correspond to stable solutions, minimizing $U[\boldsymbol{u}(\boldsymbol{x})]$, we should expect there to be a

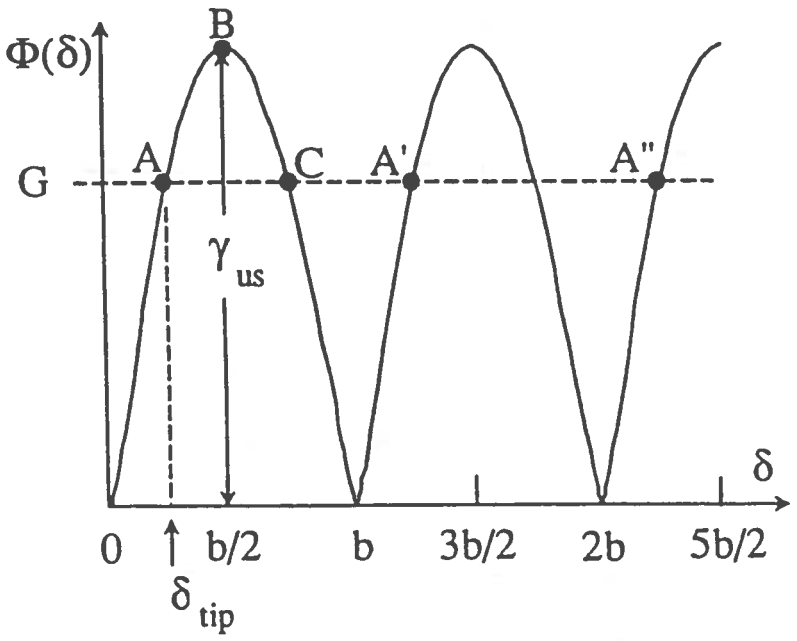

FIGURE 1.4. Solution for the slip displacement at the crack tip, for stable solution A (and A', A'', ... corresponding to one, two, or more previously emitted dislocations), and for 2D saddle-point configuration C.

saddle-point configuration between theses two states, also an extrema of $U[\boldsymbol{u}(\boldsymbol{x})]$. That saddle-point configuration evidently has a slip $\delta_{\rm tip}$ at the crack tip given by point C in Fig. 1.4, and hence we are able to calculate an important feature of the activated configuration, at least in a 2D treatment. This is of limited use because the actual saddle-point configuration, defining the activation energy for an analysis of thermally assisted dislocation nucleation when $G < \gamma_{\rm us}$, will involve a 3D elastic field associated with a localized outward protrusion of slip from the stable 2D incipient dislocation distribution corresponding to point A. Further discussion of activated states in dislocation nucleation is deferred to Section 1.13.

The same analysis as above may be followed for a crack tip loaded under mode III conditions and for which the slip direction $\boldsymbol{s}$ is in the x_3 direction, so that the emerging dislocation is of screw type. We now identify τ as σ_{23} and δ as $u_3^+ - u_3^-$. The above equations hold with $K_{\rm II}$ replaced with $K_{\rm III}$, and with $(1-\nu)$ replaced by 1, so that the nucleation condition is then

$$G \equiv K_{\rm III}^2/2\mu = \gamma_{\rm us}. \tag{1.9}$$

At this point we want to extend the results to nucleation of general dislocations, combining both edge and screw components, at crack tips under general mixed-mode loading. Also, we want to model the nucleation of dislocations in dissociated form, with first one partial dislocation nucleating,

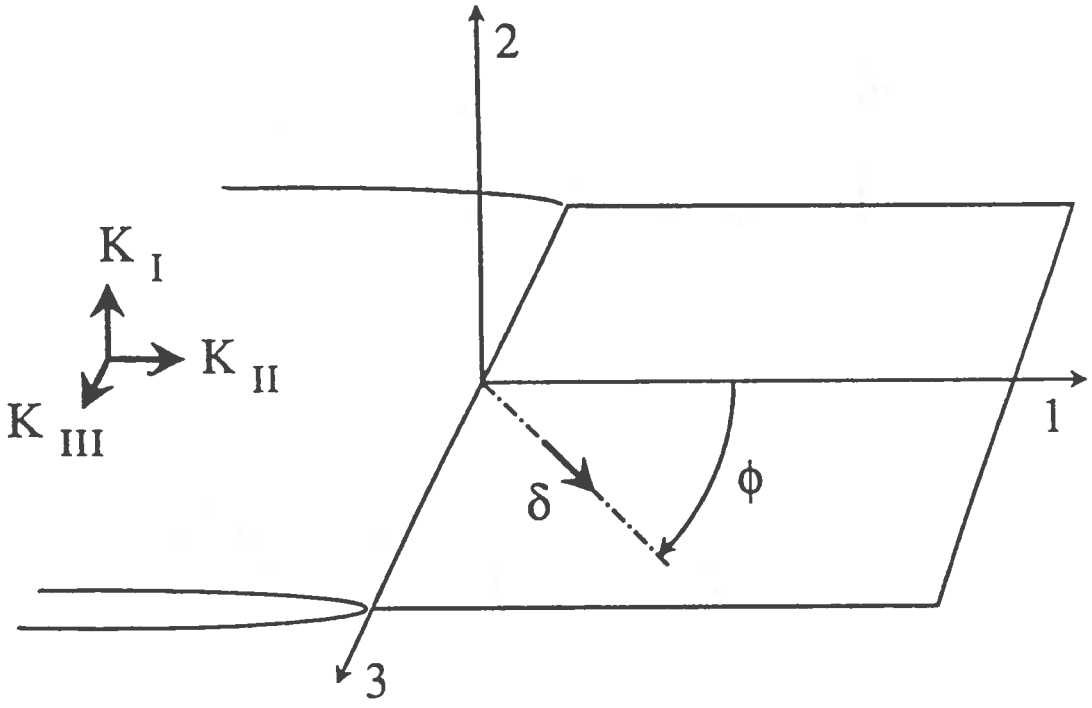

FIGURE 1.5. General mixed mode loading. Relative displacement along the slip plane assumed to follow a constrained path of pure sliding, without opening, along slip direction at angle ϕ.

leaving a faulted plane behind it, and then the remainder of the dislocation nucleating under increased external loading (e.g. , fcc metals in which partial dislocations on {111} planes are separated by stacking faults, and ordered alloys in which superlattice dislocations dissociate into partials separated by an antiphase boundary). Reasonably exact results (Rice, 1992) are given next within a "constrained-path" approximation, that is already tacit in the results presented so far.

1.4 Results for General Shear Loading, Coincident Crack and Slip Planes

Suppose now that the solid of Fig. 1.3 is loaded in combined mode I, II and III, Fig. 1.5, so that stresses on the slip plane in the absence of any relaxation would be $\sigma_{21} = K_{\rm II}/\sqrt{2\pi r}, \sigma_{22} = K_{\rm I}/\sqrt{2\pi r}, \sigma_{23} = K_{\rm III}/\sqrt{2\pi r}$. In general the displacement discontinuity on the slip plane could have components in both the 1, 2 and 3 directions, $\delta_1 = u_1^+ - u_1^-, \delta_2 = u_2^+ - u_2^-$ and $\delta_3 = u_3^+ - u_3^-$. The energy $\Phi^*(\delta_1, \delta_2, \delta_3)$ of the slip plane is now related to the stresses by $\sigma_{2\alpha} = \partial\Phi^*(\delta_1, \delta_2, \delta_3)/\partial\delta_\alpha$ and an application of the J integral paralleling that in the previous section shows that solutions of the static elastic equations for this case must have relative displacements

$(\delta_{1\text{tip}}, \delta_{2\text{tip}}, \delta_{3\text{tip}})$ at the crack tip satisfying

$$G \equiv \left[(1-\nu)\left(K_{\text{I}}^2 + K_{\text{II}}^2\right) + K_{\text{III}}^2\right]/2\mu = \Phi^*(\delta_{1\text{tip}}, \delta_{2\text{tip}}, \delta_{3\text{tip}}). \tag{1.10}$$

This condition, however, does not let us determine a nucleation condition since now there are too many degrees of freedom at the tip.

A solution can be found if we make the assumptions that the relative motion along the slip plane is pure shear so that opening $\delta_2 = 0$ (an improvement is to consider relaxed paths along which $\partial\Phi^*/\partial\delta_2 = 0$), and that a certain direction or more generally that a certain set of crystallographically equivalent directions within a slip plane are far less resistant to shear than are any other directions. Such directions would, of course, coincide with the observed slip directions $\boldsymbol{s}$, i.e., the directions of Burgers vectors $\boldsymbol{b}$. Calculations from atomic models (Yamaguchi et al., 1981; Sun et al., 1991) of slip plane energies for different directions of shear do indeed show very large differences in energy; see Section 1.9. Thus let the angle ϕ denote the angle of the easy slip direction on the slip plane, where ϕ is measured from the x_1 axis (Fig. 1.5) so that $\phi = 0$ corresponds to an edge dislocation, whereas $\phi = \pi/2$ corresponds to a screw dislocation, relative to the crack front. When there are several such directions, we shall regard ϕ as denoting the first such direction to meet the nucleation condition, derived below, under the given ratio of K_{III} to K_{II} loading.

We now make the approximation that the resistance to slip along directions other than ϕ, and the resistance to tensile opening, is so great that we can regard the relative displacement as being constrained to a pure slip path at angle ϕ, so that

$$\delta_1 = \delta\cos\phi, \delta_2 = 0, \text{ and } \delta_3 = \delta\sin\phi \tag{1.11}$$

where δ is the slip along direction ϕ. Thus if

$$\tau = \sigma_{21}\cos\phi + \sigma_{23}\sin\phi \tag{1.12}$$

denotes the resolved shear stress in the slip direction, we may assume as boundary condition along the slip plane that τ is related to δ like in Fig. 1.1(b), and that Φ of Fig. 1.1(c) is given as before as $\Phi = \int \tau d\delta$. Because of the constraint on the relative displacements, it will no longer be the case that the slip process relaxes the stress singularity at the crack tip. Thus, in addition to the K_{I}, K_{II} and K_{III} characterizing the remotely applied loading, we will also have a non-zero stress intensity factors $K_{\text{I(tip)}}$, $K_{\text{II(tip)}}$ and $K_{\text{III(tip)}}$ remaining at the crack tip at $x_1 = 0$.

Evaluation of the J integral along the path Γ_{far} gives

$$J = G \equiv \left[(1-\nu)\left(K_{\text{I}}^2 + K_{\text{II}}^2\right) + K_{\text{III}}^2\right]/2\mu \tag{1.13}$$

whereas in evaluating the contribution along Γ_{slit} we now have to include the contribution from the crack tip singularity, thus getting

$$\begin{aligned} J &= \left[(1-\nu)\left(K_{\text{I(tip)}}^2 + K_{\text{II(tip)}}^2\right) + K_{\text{III(tip)}}^2\right]/2\mu - \int_0^\infty \sigma_{2\alpha}\partial\delta_\alpha/\partial x_1 dx_1 \\ &= \left[(1-\nu)\left(K_{\text{I(tip)}}^2 + K_{\text{II(tip)}}^2\right) + K_{\text{III(tip)}}^2\right]/2\mu + \Phi(\delta_{\text{tip}}) \end{aligned} \tag{1.14}$$

where it has been noted that $\sigma_{2\alpha}\partial\delta_\alpha/\partial x_1 = \tau\partial\delta/\partial x_1 = \partial\Phi(\delta)/\partial x_1$ in view of the constraint on the slip path. The following conditions may be brought to bear: Since τ is bounded at the tip,

$$K_{\text{II(tip)}}\cos\phi + K_{\text{III(tip)}}\sin\phi = 0. \tag{1.15}$$

Also, by using the separate mode I, II and III solutions for the effect of slip on alteration of the stress intensity factors, we have

$$\begin{aligned} &[K_{\text{I}} - K_{\text{I(tip)}}, K_{\text{II}} - K_{\text{II(tip)}}, K_{\text{III}} - K_{\text{III(tip)}}] \\ &\quad = -\frac{\mu}{\sqrt{2\pi}(1-\nu)}\int_0^\infty \frac{d}{d\rho}[\delta_2(\rho), \delta_2(\rho), (1-\nu)\delta_3(\rho)]\frac{d\rho}{\sqrt{\rho}}. \end{aligned} \tag{1.16}$$

When the above constraints on the δ_α are used, this gives

$$K_{\text{I(tip)}} = K_{\text{I}}, \text{ and } (1-\nu)\sin\phi(K_{\text{II}} - K_{\text{II(tip)}}) - \cos\phi(K_{\text{III}} - K_{\text{III(tip)}}) = 0. \tag{1.17}$$

We may therefore solve for $K_{\text{II(tip)}}$ and $K_{\text{III(tip)}}$ as

$$(K_{\text{II(tip)}}, K_{\text{III(tip)}}) = \frac{(\sin\phi, -\cos\phi)}{\cos^2\phi + (1-\nu)\sin^2\phi}[(1-\nu)\sin\phi K_{\text{II}} - \cos\phi K_{\text{III}}], \tag{1.18}$$

and when we substitute these results into the two expressions for J above, and equate the expressions, one finds after a little manipulation that the slip δ_{tip} at the crack tip is given by

$$\frac{1-\nu}{2\mu}\frac{(\cos\phi K_{\text{II}} + \sin\phi K_{\text{III}})^2}{\cos^2\phi + (1-\nu)\sin^2\phi} = \Phi(\delta_{\text{tip}}). \tag{1.19}$$

This coincides with the results of the last section for mode II loading in emission of an edge ($\phi = 0$) dislocation and for mode III loading in emission of a screw ($\phi = \pi/2$). Since the maximum of Φ is γ_{us}, the nucleation criterion is therefore

$$\cos\phi K_{\text{II}} + \sin\phi K_{\text{III}} = \sqrt{\frac{2\mu}{1-\nu}[\cos^2\phi + (1-\nu)\sin^2\phi]\gamma_{\text{us}}} \tag{1.20}$$

(assuming that the left side is positive; a minus sign should precede the right side if not). The combination

$$K \equiv \cos\phi K_{II} + \sin\phi K_{III} \tag{1.21}$$

which enters the criterion has an evident interpretation as the intensity factor for the resolved shear stress along the slip direction.

Anisotropy: We may readily generalize the above discussions to take into account anisotropic elasticity (Sun and Rice, 1992). Evaluation of the J integral along the path Γ_{far} yields

$$J = G = \Lambda_{\alpha\beta} K_\alpha K_\beta \tag{1.22}$$

where $K = (K_1, K_2, K_3) = (K_{II}, K_I, K_{III})$ and $\Lambda_{\alpha\beta}$ is the appropriate matrix (derived by methods of Stroh, 1958, and Barnett and Asaro, 1972) for the anisotropic material. $\Lambda_{\alpha\beta}$ is real, symmetric, and positive definite, and is a function of the elastic constants of the material; it has the dimension of compliance and generally contains off-diagonal elements. Assume that a cohesive zone with slip $\delta(r)$ along a constrained path as above is developed to relax the singular stress field near the tip in response to the loading. There still exist residual singular stress components, which are described by the stress intensity factors $K_{\alpha(\text{tip})}, \alpha = 1, 2, 3; K_{(\text{tip})} = (K_{1(\text{tip})}, K_{2(\text{tip})}, K_{3(\text{tip})})$. The J integral evaluated along Γ_{slit} contains two contributions; one is from the crack tip singularity and the other is due to the energy $\Phi(\delta_{\text{tip}})$,

$$J = \Lambda_{\alpha\beta} K_{\alpha(\text{tip})} K_{\beta(\text{tip})} + \Phi(\delta_{\text{tip}}) \tag{1.23}$$

We define $s(\phi) = (\cos\phi, 0, \sin\phi)$ so that $\delta_\alpha(r) = \delta(r) s_\alpha(\phi)$. The anisotropic derivation for the emission criterion proceeds analogously to that of the isotropic case. Further details may be found in Sun and Rice (1992) who use $s_\alpha(\phi) K_{\alpha(\text{tip})} = 0$, corresponding to Eq. 1.15, and also the anisotropic analog of Eq. 1.16, expressing each $K_\alpha - K_{\alpha(\text{tip})}$ as a similar integral operator on $[\Lambda^{-1}]_{\alpha\beta}\delta_\beta$, to derive the nucleation condition

$$s_\alpha(\phi) K_\alpha = \sqrt{\gamma_{us} p(\phi)} \tag{1.24}$$

where we have defined $p(\phi) = [\Lambda^{-1}]_{\alpha\beta} s_\alpha(\phi) s_\beta(\phi)$.

Some tendency for dilatant opening across a lattice plane ($\delta_2 \neq 0$) must, in general, accompany shear. A particular embedded-atom model for iron, used in molecular dynamics simulations by Cheung (1990), provides an example for which the constrained-path approximation with $\delta_2 = 0$ is not so good, in that high tensile stress across slip planes at a crack tip noticeably reduce the resistance to dislocation emission (Cheung et al., 1991). These features require a more detailed formulation including numerical solution of coupled integral equations for the distribution of the δ's. The coupling of dilatant opening and shear has been analyzed based on such numerical

solutions in work by Beltz and Rice (1991, 1992a) and Sun et al. (1992) to be discussed, and confirm the conclusions of Cheung et. al (1991) for their model of α-iron.

An approximate account of such tension-shear coupling can be made by simply interpreting γ_{us} as the unstable stacking energy for *relaxed* shear, along a path with δ_2 chosen to make $\partial\Phi^*(\delta_1, \delta_2, \delta_3)/\partial\delta_2 = 0$. Such may be formally justified within an alternative "constrained path" approximation by observing that the J integral conservation applies not only to the entire elastic field but also to each crack tip mode individually. Thus, we can equate the expressions for J given by the right sides of Eqs. 1.13 and 1.14, but with the K_I and $K_{I(tip)}$ terms deleted and understanding that now α in Eq. 1.24 ranges over just 1 and 3. Hence, choosing as the constrained path that with $\partial\Phi^*/\partial\delta_2 = 0$, but restricting $\delta_1 = \delta\cos\phi$ and $\delta_3 = \delta\sin\phi$ as above, we re-derive Eq. 1.20 with γ_{us} now interpreted as the relaxed value. The procedure does a good job of describing coupled tension-shear results as will be discussed in Section 1.7.

1.5 Nucleation of Dissociated Dislocations, Coincident Crack and Slip Planes

The parts of this section based on isotropic elasticity also follow Rice (1992). Suppose that a complete lattice dislocation in a certain crystal is composed of two partial dislocations with respective Burgers vectors $\boldsymbol{b}_A$ and $\boldsymbol{b}_B$, where these share the same slip plane and are separated by a faulted portion of slip plane with energy γ_{sf} (*stacking fault* energy) per unit area. We continue with the simplification that the crack plane and slip plane are coincident as in Fig. 1.5, and make the constrained-path approximation for each partial dislocation individually. Thus partial dislocation A is created by slip δ_A from 0 to b_A along a definite direction at angle ϕ_A (the first of the different possible partial dislocation directions on the slip plane to meet the nucleation condition, under the prevailing K_{III}/K_{II} ratio), and then partial dislocation B can come into existence by slip δ_B from 0 to b_B at angle ϕ_B (taken to be the most favorable of the allowed crystal directions for continuation of slip as a second partial). For {111} planes in fcc lattices, with partials of Burgers vectors in $< 211 >$ directions summing to complete $< 11\bar{0} >$ dislocations, ϕ_B and ϕ_A differ by 60°. (Anderson (1986) previously analyzed partial dislocation nucleation within the Rice-Thomson framework.)

Energy functions Φ for the two partials are shown in Fig. 1.6. The first slip over b_A carries the energy Φ_A from zero, through the peak at γ_{us}, and to a residual state of energy γ_{sf}; the next slip starts with energy Φ_B at γ_{sf}, goes through the same peak γ_{us}, and returns to zero after slip b_B, a complete dislocation having then been formed. Let

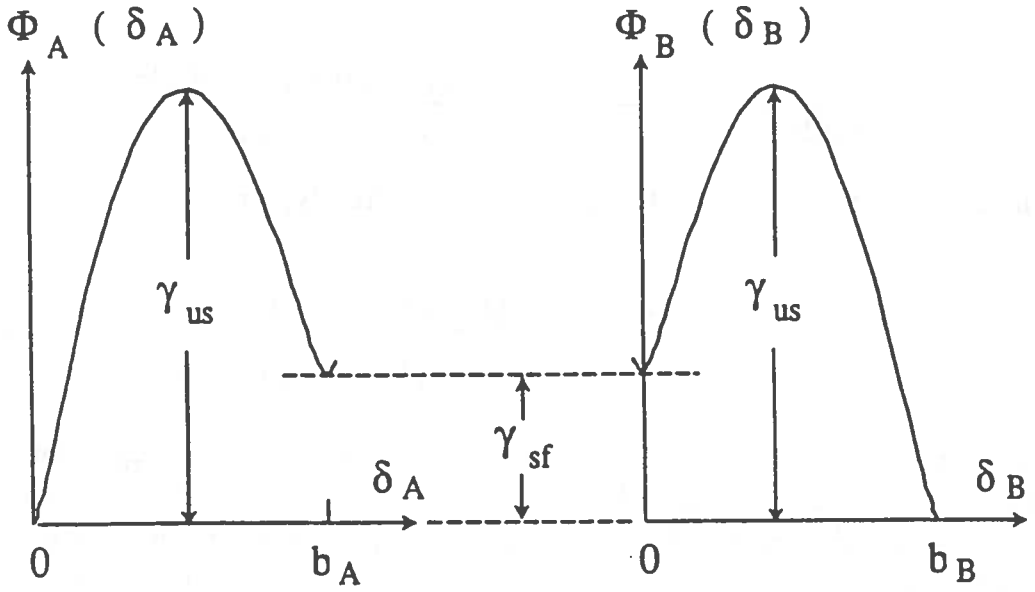

FIGURE 1.6. Energy versus slip for two partial dislocation which combine to form a complete lattice dislocation; γ_{sf} is the energy per unit area of the stacking fault.

$$K_A = K_{\rm II}\cos\phi_A + K_{\rm III}\sin\phi_A,\ K_B = K_{\rm II}\cos\phi_B + K_{\rm III}\sin\phi_B. \quad (1.25)$$

The analysis of the previous section shows that first partial nucleates when

$$K_A = K_{A\rm crit} \equiv \sqrt{\frac{2\mu}{1-\nu}[\cos^2\phi_A + (1-\nu)\sin^2\phi_A]\gamma_{\rm us}}. \quad (1.26)$$

However, the fully formed partial dislocation which emerges, of Burgers vector b_A, leaves a faulted plane of energy γ_{sf} behind it and thus is not swept indefinitely far away by the stress field but instead remains in the vicinity of the crack tip. Let r_A be the position of the core of that partial dislocation. It is determined by equilibrium between Peach-Koehler configurational forces; that due to the applied stress field $K_A/\sqrt{2\pi r}$ must balance the sum of the dislocation image force due to the presence of the stress-free crack surface (Rice and Thomson, 1974) and the force γ_{sf} tending to annihilate the fault. (We can treat this defect as a classical, singular line dislocation, without considering its spread-out core, since it will be seen that r_A is typically very large compared to b_A). Thus r_A is the (largest) root of

$$K_A b_A/\sqrt{2\pi r_A} = \gamma_{sf} + \mu b_A^2[\cos^2\phi_A + (1-\nu)\sin^2\phi_A]/4\pi(1-\nu)r_A, \quad (1.27)$$

from which one finds that

$$\frac{\mu b_A}{(1-\nu)\sqrt{2\pi r_A}} = \frac{K_A[1-\sqrt{1-(\gamma_{sf}/\gamma_{us})(K_{Acrit}/K_A)^2}}{\cos^2\phi_A + (1-\nu)\sin^2\phi_A} \tag{1.28}$$

(the combination on the left will be needed shortly) and that

$$\frac{r_A}{b_A} = \frac{(K_{Acrit}/K_A)^2[\cos^2\phi_A + (1-\nu)\sin^2\phi_A](\mu b_A/\gamma_{us})}{4\pi(1-\nu)\left[1-\sqrt{1-(\gamma_{sf}/\gamma_{us})(K_{Acrit}/K_A)^2}\right]^2}. \tag{1.29}$$

The last expression, to be used after nucleation ($K_A \geq K_{Acrit}$), defines a rapidly increasing function of K_A. It is least when $K_A = K_{Acrit}$, and then gives the position r_A to which the partial jumps just after nucleation. Later we will see estimates of $\mu b_A/\gamma_{us}$ ranging from 25 to 40 for fcc metals, and $\gamma_{sf} \approx \gamma_{us}/4$ to $\gamma_{us}/2$ seems to be representative (smaller values give larger r_A). These lead, for $\phi_A = 0$ and $\nu = 0.3$, to $r_A/b \approx 30$ to 250. This is an overestimate, in that it neglects lattice friction against motion of the partial dislocation.

The simplest way to address emission of the second partial is to note that the first partial dislocation has the effects of (i) modifying the K_{II} and K_{III} at the tip (say, to values K^*_{II} and K^*_{III}), and (ii) resetting the energy of the unslipped state from zero to γ_{sf}, Fig. 1.6, so that the peak energy to be surmounted for the instability leading to dislocation B to occur is reduced from γ_{us} to $\gamma_{us} - \gamma_{sf}$. With those factors taken into account, we can just use the result of the last section so that, at instability,

$$\begin{aligned} K^*_B &\equiv K^*_{II}\cos\phi_B + K^*_{III}\sin\phi_B \\ &= \sqrt{\frac{2\mu}{1-\nu}\left[\cos^2\phi_B + (1-\nu)\sin^2\phi_B\right](\gamma_{us}-\gamma_{sf})} \end{aligned} \tag{1.30}$$

(When we take into account the expressions for K^*_{II} and K^*_{III}, given next, the same result could be derived, alternatively, by applying the J integral, in the style of the last section, to the entire dislocated array, partial dislocation A, the associated stacking fault zone, and incipient partial dislocation B.)

The expressions for K^*_{II} and K^*_{III} are derivable from Eq. 1.26 as

$$K^*_{II} = K_{II} - \mu b_A\cos\phi_A/(1-\nu)\sqrt{2\pi r_A},\ K^*_{III} = K_{III} - \mu b_A\sin\phi_A/\sqrt{2\pi r_A}. \tag{1.31}$$

Using Eq. 1.28 for the latter terms, the quantity K^*_B entering the criterion for nucleation of the second partial is given by

$$K_B^* = K_B - \eta K_A + \eta\sqrt{K_A^2 - \frac{2\mu}{1-\nu}\gamma_{sf}[\cos^2\phi_A + (1-\nu)\sin^2\phi_A]} \quad (1.32)$$

where

$$\eta = \frac{\cos\phi_A\cos\phi_B + (1-\nu)\sin\phi_A\sin\phi_B}{\cos^2\phi_A + (1-\nu)\sin^2\phi_A}. \quad (1.33)$$

Anisotropy. The treatment of dissociated partial dislocations in an anisotropic elastic medium proceeds analogously with the isotropic case (Sun and Rice, 1992). The emission of the first partial occurs when the nucleation condition is reached in anisotropic medium,

$$K_A \equiv s_\alpha(\phi_A)K_\alpha = K_{A\text{crit}} = \sqrt{\gamma_{us}p(\phi_A)}. \quad (1.34)$$

The emitted partial dislocation is treated as a line defect; its stable equilibrium position is found from the condition that the force exerted on it vanishes:

$$f_A = K_A b_A/\sqrt{2\pi r_A} - \gamma_{sf} + f_r = 0. \quad (1.35)$$

The image force f_r on the partial dislocation itself is given by Rice (1985) as

$$f_r = -\frac{b_A^2[\Lambda^{-1}]_{\alpha\beta}s_\alpha(\phi_A)s_\beta(\phi_A)}{8\pi r_A}. \quad (1.36)$$

Hence,

$$\frac{b_A}{2\sqrt{2\pi r_A}} = \frac{K_A\left[1-\sqrt{1-(\gamma_{sf}/\gamma_{us})(K_{A\text{crit}}/K_A)^2}\right]}{p(\phi_A)} \quad (1.37)$$

The stress intensity factor is now shielded by the emitted first partial dislocation

$$K_\alpha^* = K_\alpha - b_A[\Lambda^{-1}]_{\alpha\beta}s_\beta(\phi_A)/2\sqrt{2\pi r_A}. \quad (1.38)$$

Combining Eq. 1.25 with Eq. 1.38 gives

$$K_B^* = s_\alpha(\phi_B)K_\alpha^* = K_B - \eta(\phi_B,\phi_A)K_A + \eta(\phi_B,\phi_A)\sqrt{K_A^2 - \gamma_{sf}p(\phi_A)} \quad (1.39a)$$

where

$$\eta(\phi_B,\phi_A) = \frac{[\Lambda^{-1}]_{\alpha\beta}s_\alpha(\phi_B)s_\beta(\phi_A)}{[\Lambda^{-1}]_{\alpha\beta}s_\alpha(\phi_A)s_\beta(\phi_A)} = \frac{[\Lambda^{-1}]_{\alpha\beta}s_\alpha(\phi_B)s_\beta(\phi_A)}{p(\phi_A)}. \quad (1.39b)$$

The emission of the second partial dislocation occurs when

$$K_B^* = \sqrt{(\gamma_{us}-\gamma_{sf})p(\phi_B)}. \quad (1.40)$$

The resulting nucleation criterion (now considering isotropic materials only) is a little complex to study in general, but it takes a simpler form in a special case of considerable interest for fcc metals, in which $\phi_A = 0°$ and $|\phi_B| = 60°$ (+ or - chosen according to the sign of K_{III}). The 0° partial will be the first nucleated only if $K_B < (\sqrt{4-3\nu}/2)K_A$, which is equivalent to $|K_{III}| < (\sqrt{4-3\nu}-1)K_{II}/\sqrt{3}$ or, for $\nu = 0.3$, to $|K_{III}| < 0.44K_{II}$, a condition which is now assumed to hold. The first partial nucleates when

$$K_{II} = \sqrt{2\mu\gamma_{us}/(1-\nu)} \tag{1.41}$$

and the condition for nucleation of the second, given above, now simplifies to

$$\sqrt{3}|K_{III}| + \sqrt{K_{II}^2 - 2\mu\gamma_{sf}/(1-\nu)} = \sqrt{2\mu(4-3\nu)(\gamma_{us}-\gamma_{sf})/(1-\nu)}. \tag{1.42}$$

Since this equation takes effect only after K_{II} reaches the value to nucleate the first partial, the K_{II} which enters it will always be at least as large as that of Eq. 1.26, and hence the quantity of which the square root is taken is always positive since (since $\gamma_{us} > \gamma_{sf}$).

Three possibilities exist, depending on K_{III}: (i) When K_{III} is zero or sufficiently small, K_{II} must be increased to nucleate the second partial. (ii) For $|K_{III}|$ greater than a certain limit $K_{III(sp)}$ given below, the second partial nucleates spontaneously once the first has formed; no increase in K_{II} is then required. (iii) And for $|K_{III}|$ yet larger, the analysis ultimately becomes untenable because, instead, the $|\phi| = 60°$ partial nucleates first, and we have to start from the beginning, interchanging A and B.

The greatest K_{II} to nucleate the second partial results when $K_{III} = 0$, in which case

$$K_{II} = \sqrt{2\mu[(4-3\nu)\gamma_{us} - 3(1-\nu)\gamma_{sf}]/(1-\nu)} \tag{1.43}$$

When $\nu = 0.3$ and $\gamma_{sf} = \gamma_{us}/3$, this is 55% higher than the K_{II} to nucleate the first dislocation. The required increase in K_{II} diminishes to zero when $|K_{III}| = K_{III(sp)}$, where

$$K_{III(sp)} = \sqrt{2\mu(\gamma_{us}-\gamma_{sf})/(1-\nu)}\left(\sqrt{4-3\nu}-1\right)\sqrt{3} \tag{1.44}$$

is calculated by setting K_{II} equal to that to nucleate the first partial. For the numerical values above, $K_{III(sp)}$ is 0.36 times the K_{II} to nucleate the first partial. The range of K_{III} for which there is spontaneous nucleation of the 60° partial persists up to a limit given by the same expression as for $K_{III(sp)}$ but with $(\gamma_{us} - \gamma_{sf})$ increased to γ_{us}; beyond that limit, it is the 60° partial which nucleates first.

Nucleation by the partial mechanism discussed here is considered again in the next section, where slip planes at angle $\theta \neq 0$ are considered.

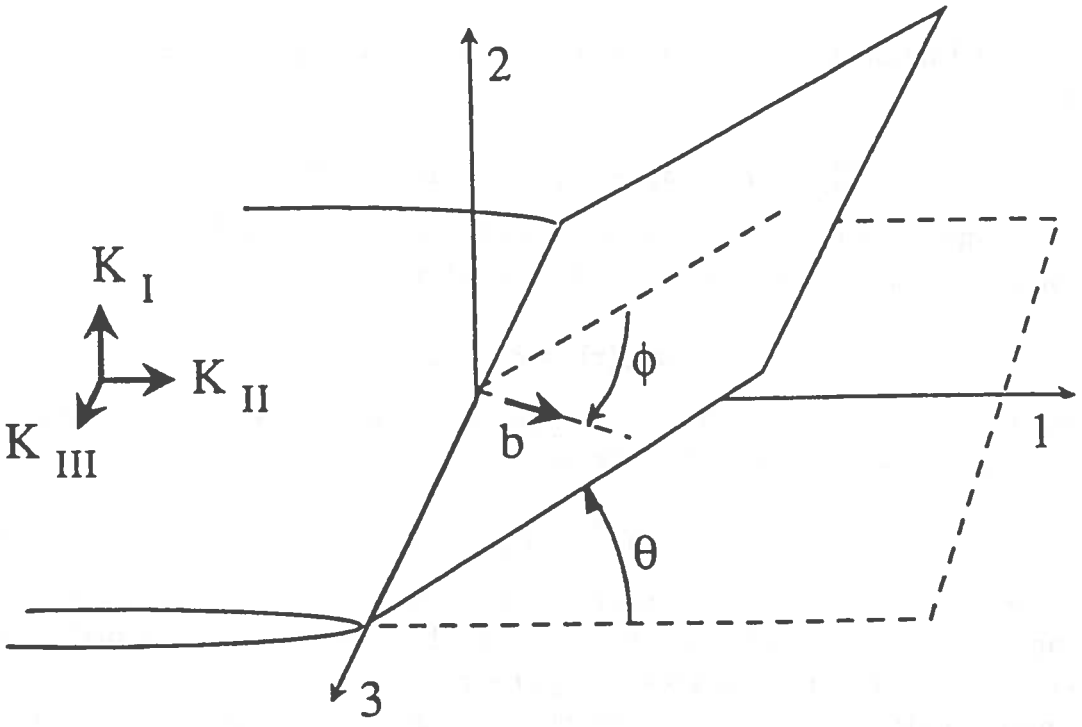

FIGURE 1.7. Slip plane inclined at angle θ with the prolongation of the crack plane; slip direction inclined at angle ϕ with the normal to the crack tip.

1.6 Approximate Nucleation Condition, Slip Plane Not Coincident with Crack Plane

In general the most highly stressed slip plane will make a non-zero angle θ relative to the crack plane, like in Fig. 1.7, and the Burgers vector direction along that plane will make an angle ϕ with a line drawn perpendicular to the crack tip, similar to Fig. 1.5.

Effective stress intensity factor concept. Rice (1992) proposed the following approximate treatment of nucleation when $\theta \neq 0$. Suppose that the solid is loaded so as to induce a general set of intensity factors $K_{\rm I}$, $K_{\rm II}$ and $K_{\rm III}$ at the crack tip. The in-plane and anti-plane shear stress components acting along the slip plane, according to the linear elastic solution, are

$$\sigma_{\theta r} = \left[K_{\rm I} f_{\rm I}(\theta) + K_{\rm II} f_{\rm II}(\theta)\right]/\sqrt{2\pi r},\ \sigma_{\theta 3} = K_{\rm III} f_{\rm III}(\theta)/\sqrt{2\pi r}. \qquad (1.45)$$

where, for the isotropic case,

$$\begin{aligned} f_{\rm I}(\theta) &= \cos^2(\theta/2)\sin(\theta/2),\ f_{\rm II}(\theta) = \cos(\theta/2)[1-3\sin^2(\theta/2)], \\ f_{\rm III}(\theta) &= \cos(\theta/2). \end{aligned} \qquad (1.46)$$

The form of these results motivate the notion of *effective* mode II and

mode III intensity factors along the slip plane at angle θ. These are defined as

$$K_{\rm II}^{\rm eff} = K_{\rm I} f_{\rm I}(\theta) + K_{\rm II} f_{\rm II}(\theta),\ K_{\rm III}^{\rm eff} = K_{\rm III} f_{\rm III}(\theta). \tag{1.47}$$

The same idea can be applied to anisotropic elasticity; the set of effective stress intensity factors $K_\alpha^{\rm eff}$ are defined by writing

$$\sigma_{\theta\alpha}(r) = K_\alpha^{\rm eff}/\sqrt{2\pi r} \tag{1.48}$$

with $\alpha = r,\ \theta,\ z$ from the general loading $\boldsymbol{K} = (K_1, K_2, K_3) = (K_{\rm II}, K_{\rm I}, K_{\rm III})$ on the main crack,

$$K_\alpha^{\rm eff} = F_{\alpha\beta}(\theta) K_\beta \tag{1.49}$$

where $F_{\alpha\beta}(\theta)$ appear in the near tip expression for $\sigma_{\theta\alpha}$ under mode β loading. Equations in the form of Eq. 1.45 and 1.47 are sufficient for orthotropic elasticity with principal axes along the x_1, x_2, x_3 system, in the following approximations, with Eqs. 1.46 then replaced by results appropriate to orthotropic elasticity, since in-plane deformation is then decoupled from anti-plane deformation.

As a simple approximation, we may now assume that the nucleation conditions derived for $\theta = 0$ in all the earlier sections of the paper apply as well to an inclined slip plane, $\theta \neq 0$, when we replace $K_{\rm II}$ and $K_{\rm III}$ in expressions earlier in the paper with the effective intensity factors $K_{\rm II}^{\rm eff}$ and $K_{\rm III}^{\rm eff}$ above. Thus the basic nucleation condition of Eq. 1.20 for a complete dislocation in an isotropic material becomes, approximately when $\theta \neq 0$,

$$\begin{aligned} &[f_{\rm I}(\theta) K_{\rm I} + f_{\rm II}(\theta) K_{\rm II}] \cos\phi + f_{\rm III}(\theta) K_{\rm III} \sin\phi \\ &\quad = \sqrt{\frac{2\mu}{1-\nu}\left[\cos^2\phi + (1-\nu)\sin^2\phi\right]\gamma_{\rm us}} \end{aligned} \tag{1.50}$$

and corresponding results are given shortly for nucleation of a dissociated dislocation.

We treat anisotropic elasticity in a parallel fashion to the isotropic case. The proper $\Lambda_{\alpha\beta}$ matrix, denoted by $\Lambda_{\alpha\beta}^{(\theta)}$ for the crack extension force G_r for a crack extending along the radial direction ($G_r = \Lambda_{\alpha\beta}^{(\theta)} K_\alpha^{\rm eff} K_\beta^{\rm eff}$, where now α, β range over r, θ, z.) is

$$\Lambda_{\alpha\beta}^{(\theta)} = R_{\alpha\gamma} \Lambda_{\gamma\delta} R_{\beta\delta} \tag{1.51}$$

where $\boldsymbol{R}$ is the rotation matrix

$$\boldsymbol{R} = \begin{bmatrix} \cos\theta & \sin\theta & 0 \\ -\sin\theta & \cos\theta & 0 \\ 0 & 0 & 1 \end{bmatrix} \tag{1.52}$$

The dislocation nucleation criterion is written the same way for $K_\alpha^{\rm eff}$ as for the coplanar case, so that

$$s_\alpha(\phi) F_{\alpha\beta}(\theta) K_\beta = \sqrt{\gamma_{\rm us} p(\phi,\theta)} \tag{1.53}$$

with

$$p(\phi,\theta) = \Lambda_{\alpha\beta}^{(\theta)^{-1}} s_\alpha(\phi) s_\beta(\phi) \tag{1.54}$$

and where now $s(\phi)$ has components $(\cos\phi,\ 0,\ \sin\phi)$ in the $(r,\ \theta,\ z)$ directions.

Exact analysis for $\theta \neq 0$. By contrast, the exact (but neglecting tension-shear coupling) route to determining a nucleation condition would involve enforcing equilibrium along the inclined slip plane, as achieved for nucleation in the edge mode in the isotropic case by satisfying the following integral equation:

$$\tau(r) = \frac{K_{\rm I} f_{\rm I}(\theta) + K_{\rm II} f_{\rm II}(\theta)}{\sqrt{2\pi r}} - \frac{\mu}{2\pi(1-\nu)} \int_0^\infty \frac{d\delta(\rho)}{d\rho} g_{11}(r,\rho;\theta)\, d\rho \tag{1.55}$$

where $g_{11}(r,\rho;\theta)$ reduces to $\sqrt{\rho/r}/(r-\rho)$ when $\theta = 0$, and where $\tau = f(\delta(r))$, e.g., $\tau = (\mu/2\pi)\sin(2\pi\Delta/b)$ where $\delta = \Delta - (h/2b)\sin(2\pi\Delta/b)$ for the Frenkel model. Solutions of Eq. 1.55 have been found in connection with the dislocation emission problem (Beltz, 1991); it has been found that there is a critical value of $K_{\rm II}^{\rm eff}$ beyond which no solutions exist, and that value is taken as the nucleation value. The critical $K_{\rm II}^{\rm eff}$ thus found has some θ dependence, in contrast to the prediction of Eq. 1.50; see below.

For pure mode I loading of an isotropic solid, in which case $G = (1-\nu)K_{\rm I}^2/2\mu$, the above approximate criterion given by Eq. 1.50 reduces to

$$G = 8\frac{1 + (1-\nu)\tan^2\phi}{(1+\cos\theta)\sin^2\theta}\gamma_{\rm us} \tag{1.56}$$

for dislocation nucleation. Figure 1.8 gives a comparison of the approximate result in Eq. 1.56 with the numerical results from the solution of Eq. 1.55 based on the Frenkel form. There is reasonable agreement and the results become identical in the limit of small θ. However, G as estimated by Eq. 1.56, based on the $K^{\rm eff}$ concept, must be reduced by 11% when $\theta = 45°$, to agree with the exact result based on Eq. 1.55, by 16% when $\theta = 55°$, and by 26% when $\theta = 90°$.

Dislocation nucleation versus cleavage. The G for dislocation emission (as given by its approximation in Eq. 1.56, in order to expedite the algebraic manipulations to follow) may be compared to

$$G = 2\gamma_s \tag{1.57}$$

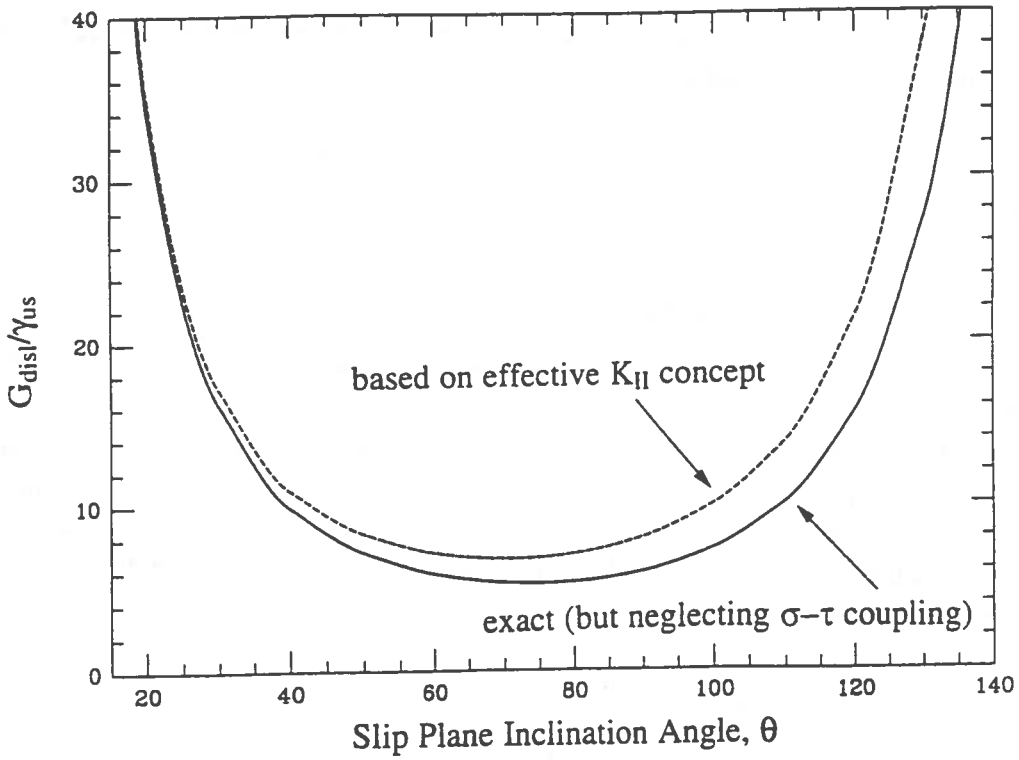

FIGURE 1.8. The critical G for dislocation nucleation versus slip plane inclination angle. The solid line is based on an exact solution (but neglects shear-tension coupling); the dashed line is calculated based on the $K^{\rm eff}$ concept.

(γ_s = surface energy) for Griffith cleavage. Hence crack tip blunting by dislocation nucleation should occur before conditions for Griffith cleavage decohesion are met if the latter G exceeds the former, which happens for the isotropic solid when

$$\frac{\gamma_s}{\gamma_{us}} > 4\frac{1+(1-\nu)\tan^2\phi}{(1+\cos\theta)\sin^2\theta}. \tag{1.58}$$

Cleavage occurs before the tip can blunt when the inequality is reversed. (Given the discussion in connection with Fig. 1.8, the number on the right side of Eq. 1.58 should be reduced by an amount ranging from approximately 10% when $\theta = 45°$ to 25% when $\theta = 90°$, if we are to have a more accurate estimate. We use the simpler formulae based on Eqs. 1.50, 1.53, and 1.56 here and in Section 1.10, except where noted otherwise).

The critical γ_s/γ_{us} ratio is, however, usually quite sensitive to deviations from pure mode I loading. For example, if x and z denote fractional shear loadings, defined by writing $K_{II} = xK_I$ and $K_{III} = zK_I$, then the inequality to be met for emission before cleavage is (Rice, 1992)

$$\frac{\gamma_s}{\gamma_{us}} > \frac{4[1+x^2+z^2/(1-\nu)][1+(1-\nu)\tan^2\phi]}{(1+\cos\theta)[\sin\theta+(3\cos\theta-1)x+2z\tan\phi]^2} \tag{1.59}$$

For a pure mode I loaded crack tip in an *anisotropic* elastic medium, the

condition of dislocation emission before crack extension is,

$$\frac{\gamma_s}{\gamma_{us}} > \frac{\Lambda_{22} s_\alpha(\phi) \Lambda^{(\theta)-1}_{\alpha\beta} s_\beta(\phi)}{2[s_\alpha(\phi) F_{\alpha 2}(\theta)]^2} \tag{1.60}$$

Equation 1.60 specializes for orthotropic elasticity, with principal axes aligned with the x_1, x_2 and x_3 coordinate system, as

$$\frac{\gamma_s}{\gamma_{us}} > \beta, \quad \text{where } \beta = \frac{[\Lambda_2 \cos^2\theta/\Lambda_1 + \sin^2\theta + \Lambda_2 \tan^2\phi/\Lambda_3]}{2 f_I(\theta)^2} \tag{1.61}$$

and this generalizes for tensile loading with some fractional shear loadings as

$$\beta = \frac{(x^2\Lambda_1/\Lambda_2 + 1 + z^2\Lambda_3/\Lambda_2)[\Lambda_2 \cos^2\theta/\Lambda_1 + \sin^2\theta + \Lambda_2 \tan^2\phi/\Lambda_3]}{2[x f_{II}(\theta) + f_I(\theta) + z f_{III}(\theta)]^2} \tag{1.62}$$

Here Λ_i ($i = 1, 2, 3$) are the diagonal components of the $\Lambda_{\alpha\beta}$ matrix discussed in connection with Eq. 1.22 and $f_I(\theta)$, $f_{II}(\theta)$ and $f_{III}(\theta)$ are the appropriate functions defined in Eq. 1.45 for a singular crack tip field but here based upon orthotropic elasticity instead of isotropic elasticity (Sun and Rice, 1992).

Consider a case of interest for bcc solids: a crack on a $\{100\}$ plane with tip along a $< 100 >$ type direction, so as to intersect a $\{110\}$ slip plane on which $< 111 >$ slip can occur. In that case, $\theta = 45°$ and $\phi = \arctan(1/\sqrt{2}) = 35.3°$. Thus, for pure mode I loading and using isotropic expressions with $\nu = 0.3$, Eq. 1.58 predicts $\gamma_s/\gamma_{us} > 6.3$ for dislocation nucleation to occur before Griffith cleavage, but according to Eq. 1.59 the required ratio reduces nearly by a half, to $\gamma_s/\gamma_{us} = 3.5$, when K_{II} and K_{III} are just 10% of K_I (i.e., $x = z = 0.1$). Implications for specific solids are discussed in Section 1.10, after reviewing some estimates of γ_{us} in Section 1.9.

Partial dislocation pair. For the nucleation of dissociated dislocations with $\theta \neq 0$, we consider a geometry of interest for fcc solids, with a crack on a $\{100\}$ plane and tip along a $< 110 >$ direction, and assume that the most stressed $\{111\}$ slip plane is that at $\theta = 54.73°$, and that the loading is such that the first partial to nucleate involves slip along the $< 211 >$ direction at $\phi_A = 0°$ with the second at $\phi_B = 60°$. Then K_A and K_B of the earlier discussion of dissociated dislocations can be replaced by K_A^{eff} and K_B^{eff}, defined like K_A and K_B in Eqs. 1.39a, 1.39b but in terms of K_{II}^{eff} and K_{III}^{eff}. For the special θ and ϕ's considered, these quantities are

$$K_A^{\text{eff}} = 0.363(K_I + 0.897 K_{II}), \; K_B^{\text{eff}} = 0.769 K_{III} + 0.5 K_A^{\text{eff}}. \tag{1.63}$$

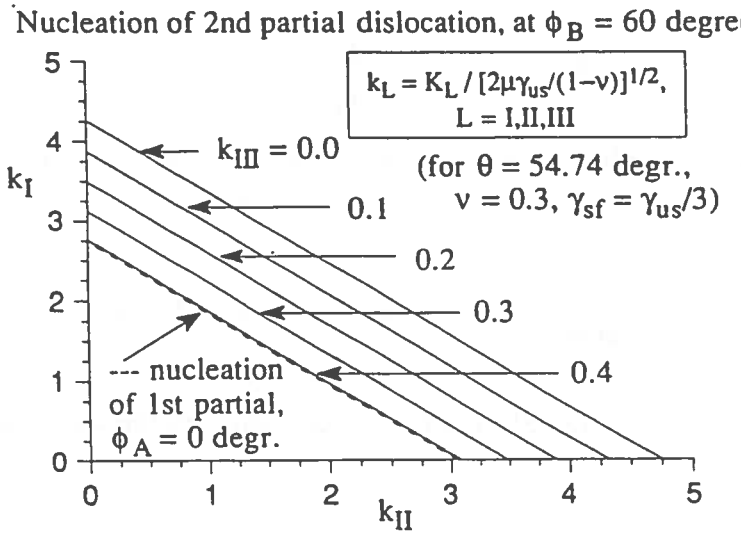

FIGURE 1.9. Combinations of $K_{\rm I}$, $K_{\rm II}$ and $K_{\rm III}$ for nucleation of the second of two partial dislocations in a fcc crystal with crack on {100} plane, with tip along $< 110 >$ direction so that the relevant {111} slip plane is at $\theta = 54.74°$; the first partial is assumed to nucleate with $\phi = 0°$ and the second with $\phi = 60°$.

It is assumed that $K_{\rm II} \geq 0$ and $K_{\rm III} \geq 0$. If not, the same phenomena will occur relative to $\theta = -54.73°$ if $K_{\rm II} < 0$ and to $\phi_B = -60°$ if $K_{\rm III} < 0$, so $K_{\rm II}$ and $K_{\rm III}$ here can be interpreted as $|K_{\rm II}|$ and $|K_{\rm III}|$.

Reading from the earlier results, interpreted approximately in terms of the effective shear stress intensity factors, the 0° partial will indeed be the first to nucleate when $K_{\rm III} < 0.179(K_{\rm I} + 0.897K_{\rm II})$, and the nucleation condition (from Eq. 1.26) for that first partial is

$$K_{\rm I} + 0.897K_{\rm II} = 2.75\sqrt{2\mu\gamma_{\rm us}/(1-\nu)}. \tag{1.64}$$

This is shown as the dashed line in Fig. 1.9, which is analogous to the mixed mode nucleation diagrams of Lin and Thomson (1986). The nucleation condition for the second partial, at $\phi_B = 60°$, is then, from Eqs. 1.30, 1.32, 1.33, 1.63,

$$0.769K_{\rm III} + 0.5\sqrt{[0.363(K_{\rm I} + 0.897K_{\rm II})]^2 - \frac{2\mu}{1-\nu}\gamma_{\rm sf}} = \sqrt{\frac{(4-3\nu)\mu}{2(1-\nu)}(\gamma_{\rm us} - \gamma_{\rm sf})}. \tag{1.65}$$

For pure mode I loading, this is

$$K_{\rm I} = 2.75\sqrt{2\mu[(4-3\nu)\gamma_{\rm us} - 3(1-\nu)\gamma_{\rm sf}]/(1-\nu)}, \tag{1.66}$$

or $K_I = 4.26\sqrt{2\mu\gamma_{us}/(1-\nu)}$ when $\nu = 0.3$ and $\gamma_{sf} = \gamma_{us}/3$. The combined loading result is plotted in Fig. 1.9, based on $\nu = 0.3$ and $\gamma_{sf} = \gamma_{us}/3$, for various values of K_{III}. The nucleation condition is extremely sensitive to K_{III}: While the numerical factor 2.75 in Eq. 1.64 above increases to 4.26 for nucleation of the second partial when $K_{III} = 0$, that factor is reduced back to 2.75 (so that there is spontaneous nucleation of the second partial) when K_{III} is increased so that an analogously defined numerical factor for K_{III} reaches only 0.404.

Emission of partial dislocations before cleavage. From Eqs. 1.64 and 1.57, the first partial will nucleate before the Griffith cleavage condition is met, under pure mode I loading of the fcc configuration considered, if $\gamma_s/\gamma_{us} > 3.8$. Since $\phi_A = 0$, this result is insensitive to mode III loading, at least as long as $|K_{III}| < 0.179K_I$ so that the $\phi = 0°$ partial is actually the first to nucleate. If there is also a 10% mode II loading ($x = 0.1$), the inequality changes somewhat, to $\gamma_s/\gamma_{us} > 3.2$.

Under pure mode I loading, the second partial, and hence the complete fcc dislocation, nucleates before Griffith cleavage if, from Eqs. 1.66 and 1.57,

$$\gamma_s/\gamma_{us} > 3.8[4 - 3\nu - 3(1-\nu)\gamma_{sf}/\gamma_{us}], \tag{1.67}$$

which is $\gamma_s/\gamma_{us} > 9.1$ when $\nu = 0.3$ and $\gamma_{sf} = \gamma_{us}/3$. However, as anticipated from the discussion above, this result is extremely sensitive to small shear mode contributions, especially in mode III. Thus for loading with K_{II} and K_{III} both 10% of K_I, and with $\nu = 0.3$ and $\gamma_{sf} = \gamma_{us}/3$, the inequality becomes $\gamma_s/\gamma_{us} > 4.2$, so that there is a reduction to less than a half of the γ_s/γ_{us} value required for nucleation prior to cleavage under pure mode I loading.

Because of the strong sensitivity to shear loadings illustrated here, and in the earlier bcc discussion, it should rather commonly be the case that dislocations emerge from (nominally) tensile loaded cracks in solids which violate the γ_s/γ_{us} requirement for ductility under pure tensile loading by as much as, say, a factor of 2.

Anisotropy: We consider emission of paired partial dislocations in fcc metals within the anisotropic elasticity framework, adopting the same crack geometry and slip plane as in the isotropic case. That is, the crack is on the (001) plane growing along the $[\bar{1}10]$ direction; the slip plane which contains the [110] crack front and which is the easiest plane on which slip can occur under tensile loading, is the $(1\bar{1}1)$ plane. The slip plane makes an angle of $\theta = 54.7°$ with the crack plane.

We consider the paired partials, $(1/6)\,[\bar{1}12]$ as the first Shockley partial and $(1/6)\,[\bar{2}\bar{1}1]$ as the second partial. The condition for the first partial emission under pure mode K_I loading is expressed by Eq. 1.61, and the resulting parameter β is listed in Table 1.1 for fcc metals. The first partial slip is along the r direction, $\phi_A = 0°$.

The anisotropic case can be discussed similarly to the isotropic for emission of the second partial, based on the $K_\alpha^{\rm eff}$ concept and the appropriate $\Lambda_{\alpha\beta}^{(\theta)}$ matrix for that inclined slip plane and Eq. 1.34 to 1.40 of the last section for partial dislocation when $\theta = 0°$. For the same geometry as in the isotropic case, $\phi_A = 0°$, and $\phi_B = 60°$, $\eta(\phi_A, \phi_B) = 1/2$ from Eq. 1.39b. The nucleation condition for the second partial, after Eq. 1.40, is thus

$$(\sqrt{3}/2)K_z^{\rm eff} + (1/2)\sqrt{K_r^{\rm eff\,2} - \gamma_{\rm sf} p(\phi_A, \theta)} = \sqrt{(\gamma_{\rm us} - \gamma_{\rm sf}) p(\phi_B, \theta)} \quad (1.68)$$

For pure tensile loading, the loading required for nucleation of the second partial is thus

$$K_{\rm I} = \sqrt{4(\gamma_{\rm us} - \gamma_{\rm sf}) p(\phi_B, \theta) + \gamma_{\rm sf} p(\phi_A, \theta)}/f_{\rm I}(\theta) \quad (1.69)$$

The condition of second partial emission before Griffith cleavage condition is met is again expressed in the inequality form

$$\frac{\gamma_s}{\gamma_{\rm us}} > \beta \quad (1.70)$$

where now

$$\beta = \frac{\Lambda_{22}[4(1 - \gamma_{\rm sf}/\gamma_{\rm us}) p(\phi_B, \theta) + \gamma_{\rm sf} p(\phi_A, \theta)/\gamma_{\rm us}]}{2[f_{\rm I}(\theta)]^2} \quad (1.71)$$

The equation above further simplifies, when taking $\gamma_{\rm sf}/\gamma_{\rm us} = 1/3$ as in estimates for the isotropic case, to

$$\beta = \frac{\Lambda_{22}[8p(\phi_B, \theta) + p(\phi_A, \theta)]}{6[f_{\rm I}(\theta)]^2} \quad (1.72)$$

The values for various fcc metals are listed in Table 1.1 with $\gamma_{\rm sf}$ taken as $\gamma_{\rm us}/3.7$.

1.7 Effects of Tension Across the Slip Plane; Shear-Tension Coupling

The procedures for determining G discussed thus far have not explicitly considered effects of tensile stress across the slip plane. Cheung et al. (1990), and earlier Argon (1987), have argued that shear softening by high tensile stress is a critical element in dislocation nucleation. We can model such effects by broadening the framework to include coupled shear and tension (Beltz and Rice, 1991, 1992a). In the calculations to be discussed, the tensile stress across the slip plane, in the absence of slip, is assumed to follow the well-known fit, with energy proportional to $-(L + \Delta_\theta)\exp(-\Delta_\theta/L)$, to the universal bonding correlation of Rose et. al. (1983). Here Δ_θ is the

opening and Δ_r the shear displacement between neighboring atomic planes. The parameter L has been suggested as scaling with the Thomas-Fermi screening length; here it can be loosely interpreted as the characteristic length associated with the decohesion process (σ reaches its maximum, at $\Delta_r = 0$, when $\Delta_\theta = L$). An analytical form for the shear and normal stress on a slip plane as functions of the relative atomic shear Δ_r and opening Δ_θ, which combines the Frenkel relation and the universal bonding correlation, has been proposed by Beltz and Rice (1991, 1992a) and is given by the following equations:

$$\tau = A(\Delta_\theta) \sin\left(\frac{2\pi\Delta_r}{b}\right) \tag{1.73a}$$

$$\sigma = [B(\Delta_r)\Delta_\theta - C(\Delta_r)]\, e^{-\Delta_\theta/L} \tag{1.73b}$$

where

$$A(\Delta_\theta) = \frac{\pi\gamma_{us}^{(u)}}{b} - \frac{2\pi\gamma_s}{b}\left\{q\left(1 - e^{-\Delta_\theta/L}\right) - \left(\frac{q-p}{1-p}\right)\frac{\Delta_\theta}{L}e^{-\Delta_\theta/L}\right\} \tag{1.74a}$$

$$B(\Delta_r) = \frac{2\gamma_s}{L^2}\left\{1 - \left(\frac{q-p}{1-p}\right)\sin^2\left(\frac{\pi\Delta_r}{b}\right)\right\} \tag{1.74b}$$

$$C(\Delta_r) = \frac{2\gamma_s}{L}\frac{p(1-q)}{1-p}\sin^2\left(\frac{\pi\Delta_r}{b}\right) \tag{1.74c}$$

and

$$q = \frac{\gamma_{us}^{(u)}}{2\gamma_s},\ p = \frac{\Delta_\theta^*}{L} \tag{1.75}$$

and where Δ_θ^* is the value of Δ_θ after shearing to the state $\Delta_r = b/2$ under conditions of zero tension, $\sigma = 0$ (i.e., relaxed shearing). The form of these equations is consistent with the existence of a potential $\Psi = \Psi(\Delta_r, \Delta_\theta)$, with $\sigma = \partial\Psi/\partial\Delta_\theta$ and $\tau = \partial\Psi/\partial\Delta_r$, and Ψ is the same as the potential introduced by Needleman (1990) when $p = q$. Here $\gamma_{us}^{(u)}$ denotes the unstable stacking energy for *unrelaxed* shear ($\Delta_\theta = 0$). It has been determined that coupling effects may be approximated by using a modified form of γ_{us}, denoted $\gamma_{us}^{(u*)}$ and defined as $\int \tau d\Delta_r$ along the path from $\Delta_r = 0$ to $\Delta_r = b/2$ with Δ_θ *fixed* at the value Δ_θ^*. In terms of the above quantities $\gamma_{us}^{(u*)}$ may be written as

$$\frac{\gamma_{us}^{(u*)} - \gamma_{us}^{(u)}}{\gamma_{us}^{(u)}} = -\frac{(p^2 - q)e^{-p} + q(1-p)}{q(1-p)} \tag{1.76}$$

The parameter p, referred to here as the "dilation parameter," as well as q and L/b have been estimated so as to be consistent with results of various

TABLE 1.1. Partial Dislocation Nucleation; Anisotropic Formulation
fcc metals [(001) cracks growing along $[\bar{1}10]$ with slip on $(1\bar{1}1)$ plane, (1/6) $[\bar{1}12]$ as the first partial and (1/6) $[\bar{2}11]$ as the second partial]. The β value, for the inequality $\gamma_s/\gamma_{us} > \beta$ in order that the first partial and second partial be emitted before the Griffith cleavage condition is reached under pure tensile loading, is listed.
These β values are based on the K_{eff} concept.

Solid	β for first partial emission	β for second partial emission*
isotropic, $\nu = 0.3$	3.8	9.1
Ag	5.33	11.1
Al	4.05	9.23
Au	5.04	11.0
Cu	5.55	11.8
Ir	4.44	10.85
Ni	5.29	12.0
Pb	5.52	10.8
Pt	4.35	9.33

TABLE 1.2. Comparison of the Critical G for Emission on Inclined Slip Planes

System	$G/\gamma_{us}^{(**)}$ (based on K_{II}^{eff})	$G/\gamma_{us}^{(**)}$ (slip only; no coupling)	$G/\gamma_{us}^{(**)}$ (full $\sigma-\tau$ coupling)	% Red., (K_{II}^{eff} to full $\sigma-\tau$ coupling)
EAM-Fe (bcc)				
$(p = 0.214, q = 0.158, L/b = 0.204)$				
$\theta = 45°$	9.37	8.34	7.80	17%
$\theta = 90°$	8.00	5.92	6.33	21%
EAM-Al (fcc)				
$(p = 0.140, q = 0.0855, L/b = 0.279)$				
$\theta = 54.7°$	7.61	6.43	6.33	17%
$\theta = 90°$	8.00	5.92	6.21	22%
EAM-Ni (fcc)				
$(p = 0.132, q = 0.0879, L/b = 0.271)$				
$\theta = 54.7°$	7.61	6.43	6.27	18%
$\theta = 90°$	8.00	5.92	6.15	23%

embedded atom models by Sun et al. (1992). Representative values are shown in Table 1.2. For general in-plane loadings, the equilibrium discussed in connection with Eq. 1.55 for an incipient dislocation of edge type is now described by a pair of coupled integral equations:

$$\tau(\Delta_r, \Delta_\theta) = \frac{K_I f_I(\theta) + K_{II} f_{II}(\theta)}{\sqrt{2\pi r}} - \frac{\mu}{2\pi(1-\nu)} \int_0^\infty g_{11}(r,\rho;\theta) \frac{d\delta_r(\rho)}{d\rho} d\rho - \frac{\mu}{2\pi(1-\nu)} \int_0^\infty g_{12}(r,\rho;\theta) \frac{d\delta_\theta(\rho)}{d\rho} d\rho \qquad (1.77a)$$

$$\sigma(\Delta_r, \Delta_\theta) = \frac{K_I f_I^\sigma(\theta) + K_{II} f_{II}^\sigma(\theta)}{\sqrt{2\pi r}} - \frac{\mu}{2\pi(1-\nu)} \int_0^\infty g_{21}(r,\rho;\theta) \frac{d\delta_r(\rho)}{d\rho} d\rho - \frac{\mu}{2\pi(1-\nu)} \int_0^\infty g_{22}(r,\rho;\theta) \frac{d\delta_\theta(\rho)}{d\rho} d\rho \qquad (1.77b)$$

where the functions $f^\sigma(\theta)$ relate the applied stress intensity factors to the normal stress $\sigma = \sigma_{\theta\theta}$ across a slip plane in the linear elastic solution, and where $\delta_r = \Delta_r - h\tau/\mu$, $\delta_\theta = \Delta_\theta - L^2\sigma/2\gamma_s$. We show results for three choices of the parameters p, q, and L/b. Each set has been chosen to approximately fit the potential $\Psi(\Delta_r, \Delta_\theta)$ associated with Eqs. 1.68, 1.69 to the corresponding potential found numerically by atomic calculations (Sun, 1991), using the Embedded Atom Method, for the block-like relative motion of one half of a crystal relative to the other by shear and opening across a lattice slip plane. This has been done for $\{110\} < 111 >$ slip in an EAM model of α-Fe and also for $\{111\} < 211 >$ slip, corresponding to emission of the first Shockley partial, in EAM models of Al and Ni; some further details relating to the atomic calculations are given in the next section.

Figures 1.10(a), 1.10(b), and 1.10(c) show results for pure edge dislocation nucleation for the three different materials when the slip plane is taken to be coplanar with the crack plane (i.e., $\theta = 0$). The critical G for emission or cleavage, whichever occurs first along the slip plane, is plotted as a solid line as a function of the loading phase angle Ψ, defined such that $\tan\Psi = K_{II}/K_I$ (e.g., pure shear corresponds to $\Psi = 90°$ and pure tension corresponds to $\Psi = 0°$). The Griffith condition $G = 2\gamma_s$ is reproduced at small Ψ. Figure 1.10(a) is for the slip system $\{110\} < 111 >$ in iron, and Figs. 1.10(b) and 1.10(c) are for the slip system $\{111\} < 211 >$ in aluminum and nickel, respectively (i.e., the emission of the first Shockley partial). The dashed line in each figure gives results when no tension

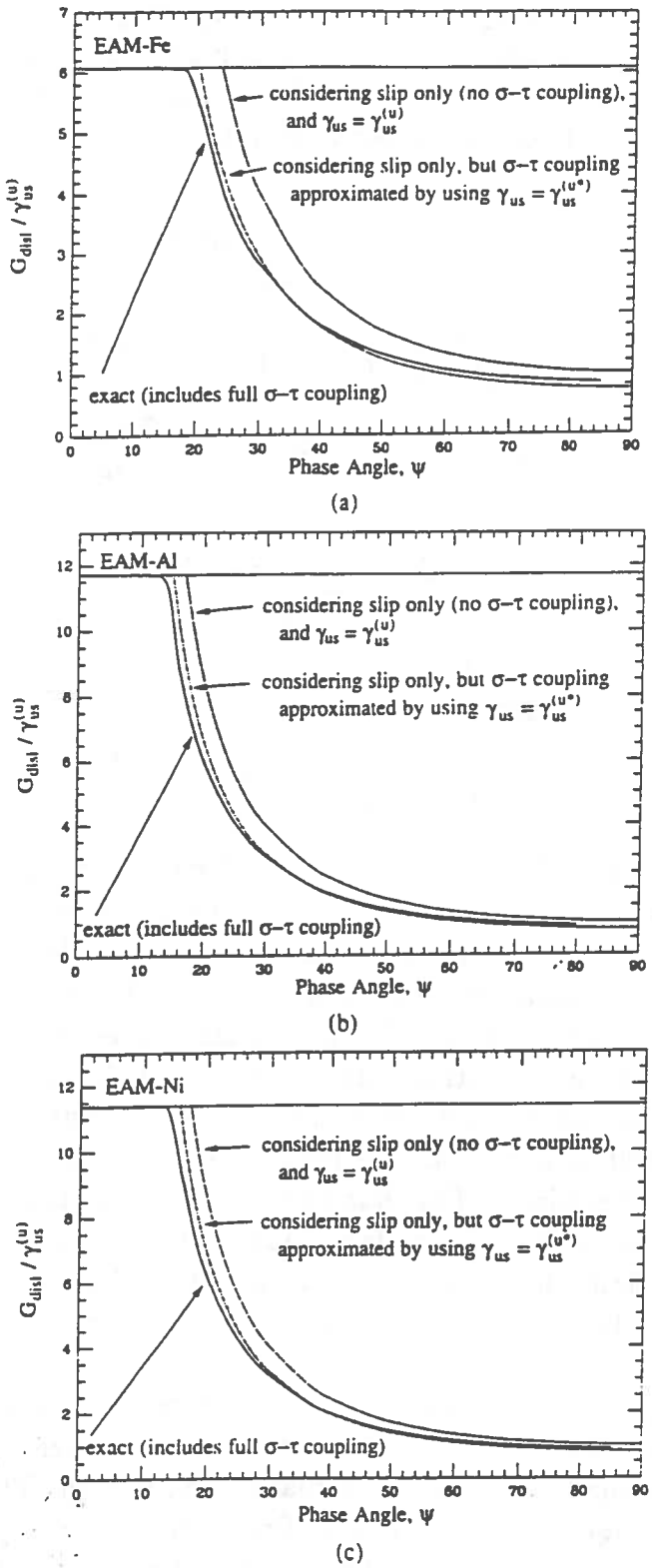

FIGURE 1.10. (a) The critical G for emission of a full dislocation in (EAM) α-Fe versus the loading phase angle ($\tan \Psi = K_{II}/K_I$) when the slip plane is coplanar with the crack plane ($\theta = 0$). The solid line is based on an exact numerical solution of Eqs. 1.77 which takes into account coupling between tension and shear. The dashed line is based on a calculation which only considers slip, for which the exact result is then given by Eq. 1.8, and uses $\gamma_{us} = \gamma_{us}^{(u)}$. The dash/dotted line is based on the same calculation but with $\gamma_{us} = \gamma_{us}^{(u^*)}$. (b) and (c) are the same except they are for a partial dislocation in EAM-Al and EAM-Ni, respectively.

effects are included and we consider slip only. It corresponds to setting $\Delta_\theta = \delta_\theta = 0$ and ignoring the second integral equation, in which case the solution for the nucleation condition is exactly (since $\theta = 0$) that given by Eq. 1.8 with γ_{us} identified as $\gamma_{us}^{(u)}$, the unrelaxed value. The alternating dash/dot line in each figure corresponds to Eq. 1.8 with γ_{us} identified as the modified value, $\gamma_{us}^{(u*)}$, which will be seen to provide an approximate way of dealing with coupled shear and tension effects.

For all three cases, the approximation based on simply using $\gamma_{us}^{(u*)}$ is seen to be quite good when $\theta = 0$. It is less accurate when used, in conjunction with the K^{eff} concept of Section 1.6, to deal with typical cases of interest when $\theta \neq 0$, although the largest source of error is with the K^{eff} concept, as already discussed in connection with Fig. 1.8. Table 1.2 gives comparisons of the G values for a few special cases in the same materials involving inclined slip planes. The first column gives G based on the K^{eff} concept, and the second column gives G as predicted by the numerical solution of Eq. 1.55, i.e., only slip is taken into account. For both of these methods, γ_{us} is identified with $\gamma_{us}^{(u*)}$. The third column gives G as calculated from the numerical solution of Eqs. 1.77a and 1.77b, in an analysis which thus fully considers tension-shear coupling; the results are normalized to $\gamma_{us}^{(u*)}$ as given by Eq. 1.76. The reduction of G, from its value given by the K^{eff} concept, that occurs when coupling effects are taken into account is expressed as a percentage in this table; these effects appear to be appreciable: reductions of the critical G for emission are in the range of 17–18% for $\theta = 45°$ or 54.7° and 21–23% for $\theta = 90°$.

Inspection of the final two columns of Table 1.2 shows, however, that the approximation based on $\gamma_{us}^{(u*)}$ is also quite good for inclined slip planes, *assuming that the approximation uses the G based on the calculation which considers slip only.* The error in this approximation shows no clear trend; and ranges from ±1.6% to ±6.9%. This justifies the earlier statement that the major source of error in this approximation for inclined slip planes is due to the K^{eff} concept. These considerations are important when addressing the ductile versus brittle behavior of crystals, as will be taken up in Section 1.10.

1.8 Width of the Incipient Dislocation Zone at Instability

The width of the incipient dislocation zone at the moment of instability is also of interest. It will be seen that the width at a crack tip is, at the moment of instability, a moderately broad feature compared to a lattice spacing, thus making more appropriate the use of the Peierls concept. Indeed, Peierls (1940) laments towards the end of his paper that the dislocation core size which he calculated, for an isolated dislocation in an otherwise

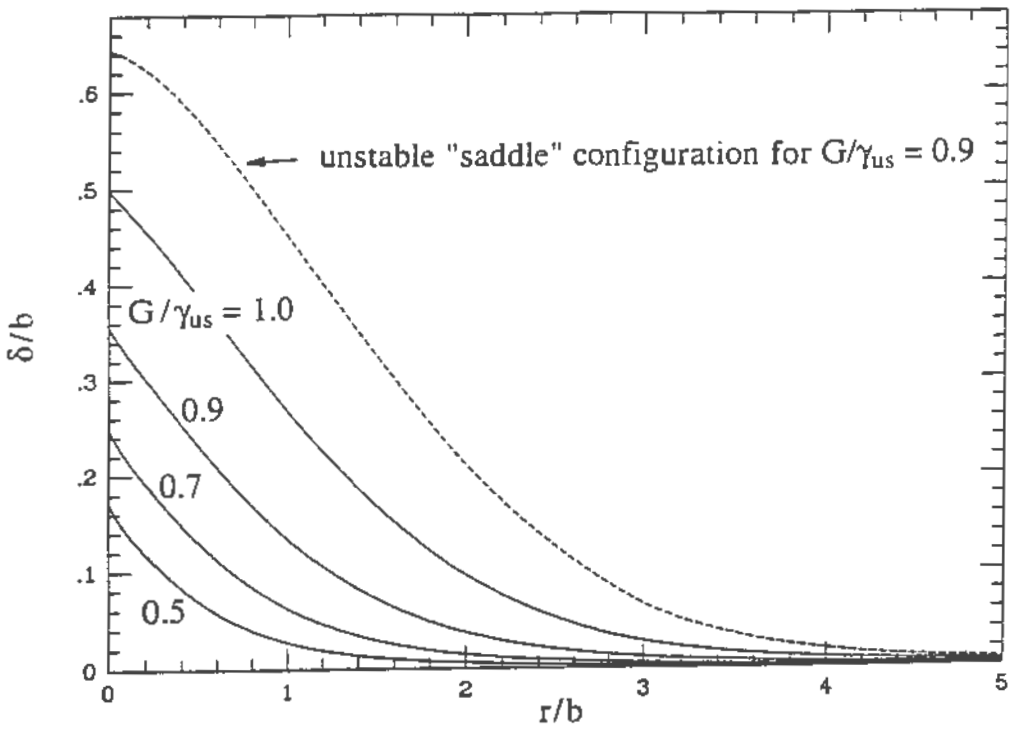

FIGURE 1.11. Displacement profiles at various levels of applied energy release rate up to instability for a pure mode II shear crack in an isotropic material, assuming $\nu = 0.3$ and $h = b$. The dashed line is an unstable "saddle" configuration corresponding to a load of $0.9G_{\text{crit}}$.

perfect lattice, was sufficiently narrow compared to b that the concept of a continuously distributed core displacement, amenable to analysis by continuum elasticity, becomes problematical. The results for nucleation at a crack tip appear to be more favorable.

The core width at instability can be estimated from a full numerical solution of Eq. 1.55. Such solutions have been carried out by Beltz and Rice (1991) based on a $\tau = f(\delta)$ relation obtained from the Frenkel sinusoid for the case when $\theta = 0$ and various ratios of applied K_{I} and K_{II}; here we consider the case when $K_{\text{I}} = 0$, i.e., pure shear. Solutions are shown for $h = b$ and $\nu = 0.3$ in Fig. 1.11 at various load levels up to instability. The characteristic width over which $\delta(r)$ is appreciable is roughly $(2 - 3)b$.

To quantitatively compare core widths, we may make a comparison with Peierls' width, also based on the Frenkel form, of $h/2(1 - \nu)$ (Hirth and Lothe, 1982) for an isolated dislocation. This width is the distance over which τ diminishes from its peak value to its unstable zero value at $\delta = \Delta = b/2$, i.e., $b/4 < \Delta < b/2$, corresponding to $(\pi - 2)b/4\pi < \delta < b/2$. The half width for an isolated dislocation (assuming $b = h$, to be consistent with the conditions under which the integral equation is solved) is about $0.71b$; applying the same definition to the incipient dislocation (loaded at instability) gives a half-width of approximately $2.05b$, an increase by a factor of 2.9.

Nabarro (1947) solved the problem corresponding to that of Peierls for the case of two coplanar dislocations of opposite sign, attracting one another and subjected to a stress just sufficing to hold them in unstable equilibrium, in an otherwise perfect lattice. This is a nice analog of the problem of dislocation nucleation from a crack tip, particularly when we recall the Rice and Thomson (1974) result that the self force on a line dislocation at distance r from a crack tip is the attractive force caused by an oppositely signed dislocation lying at distance $2r$ away in an uncracked, otherwise perfect solid. Like what we infer here, Nabarro's (1947) results show that the core widens considerably from the Peierls size as the two dislocations are brought close to one another.

1.9 Estimates of the Unstable Stacking Energy, γ_{us}

Frenkel estimates: The simplest estimate of γ_{us} is based on the Frenkel sinusoid. This is rewritten here, for shear relative to atomic planes spaced by h, as

$$\tau = (\mu_{slip} b_{eff}/2\pi h)\sin(2\pi\Delta/b_{eff}) \tag{1.78}$$

to emphasize that the modulus, μ_{slip}, should be that for shear relative to the slip system, and given as $\mu_{slip} = (c_{11} - c_{12} + c_{44})/3$ for the fcc and bcc crystal slip systems considered here. Also the Burgers vector is replaced by an effective value, b_{eff}, to emphasize that in some cases the $\Delta(= b_{eff}/2)$ at maximum energy γ_{us}, i.e., at the unstable zero of τ, may not coincide with $b/2$. Thus

$$\gamma_{us(Frenkel)} = \mu_{slip} b_{eff}^2/2\pi^2 h \tag{1.79}$$

and there is no distinction to be made in this simple model between relaxed ($\sigma = 0$) and unrelaxed $\Delta_\theta = 0$) values. The result is shown in the dimensionless form $\gamma_{us(Frenkel)}/\mu_{slip} b$ as the first numerical column of Table 1.3 for partial dislocation on {111} planes in fcc solids and for complete dislocation on two common slip planes, {110} and {211}, in bcc solids. For the fcc and first bcc case $b_{eff} = b$ (where, consistently with earlier use, in the fcc case b corresponds to that of a Shockley partial). However, the Frenkel model is expected to give a poor representation of the $\tau = F(\Delta)$ relation for shear on the {211} plane in bcc (Vitek et al., 1972), especially for shear in the twinning direction on that plane, in which direction it is possible that slip energy Φ (or Ψ) has a local maximum corresponding to the twinned structure, as it climbs towards γ_{us}. The geometry of shear in the anti-twinning direction (Paxton et al., 1991) seems somewhat simpler and the Frenkel model might apply approximately with the Δ at γ_{us} re-

duced from $b/2$ to a value perhaps as low as $b/3$. Thus, for that case, b_{eff} is given a range $2b/3$ to b in Table 1.3, resulting in the $\gamma_{\text{us(Frenkel)}}$ range shown.

To go beyond these simple estimates we require models of atomic potentials in solids. In principle, the energy γ_{us} could be determined by a quantum mechanical computations, based on (electron) density functional theory in the local density approximation, of the ground state energy of the configuration for which one half of a lattice is rigidly shifted relative to the other along a slip plane, so as to coincide with the unstable stacking (like in configuration (d) in Fig. 1.2). The analysis of such atomic geometries seems consistent with the present level of development of density functional computations.

For the present it is necessary to be content with empirical atomic models. A recently developed class of these, going beyond pair potentials and thus avoiding Cauchy symmetry of crystal moduli, have been formulated within the *Embedded Atom Method* (Daw and Baskes, 1984) and have found extensive applications to solid state phenomena, including interfacial structure and deformation and fracture. A few results for γ_{us} based on such models are now summarized.

Embedded Atom Models: Such embedded atom models as have been introduced seem to lead to lower estimates of γ_{us} than does the Frenkel model. The results will be different for direct shear with no relaxation in the direction normal to the slip plane (the most commonly available case), and for relaxed shear for which the lattice spacing h is allowed to dilate during shear so as to keep zero normal stress. As we have seen, the latter case is the most relevant one for use in the simplified nucleation criterion (e.g., Fig. 1.10 and Table 1.2, comparing 2nd and 3rd columns).

Cheung (1990) (see also Cheung et al., 1991) employed an embedded atom model for bcc Fe and, from plots of his potential for $\{110\} < 111 >$ shear, we may infer that $\gamma_{\text{us(EAM)}} = 0.44$ (relaxed) to 0.52 (unrelaxed) J/m^2. The dimensionless $\gamma_{\text{us(EAM)}}/\mu_{\text{slip}}b$ is entered for Fe in the second numerical column of Table 1.3 where, here and next, μ_{slip} is the slip system shear modulus that is consistent with the embedded atom potentials used.

Sun et al. (1991, 1992) have done similar calculations based on embedded atom models for $\{111\} < 211 >$ shears forming partial dislocation in fcc metals. These are for the respective cases of Al modeled by the potentials of Hoagland et al. (1990) and Foiles and Daw (1987), and Ni by the potentials of Foiles et al. (1986). These unrelaxed results are $\gamma_{\text{us(EAM)}} = 0.092 J/m^2$ for Al and $0.260 J/m^2$ for Ni; both numbers correspond to nearly the same $\gamma_{\text{us(EAM)}}/\mu_{\text{slip}}b$, of 0.026 as entered in Table 1.3. Relaxed $\gamma_{\text{us(EAM)}}$ values are also shown and are 87% and 86% that of the unrelaxed $\gamma_{\text{us(EAM)}}$ for Ni and Al, respectively. This is close to the 85% of unrelaxed $\gamma_{\text{us(EAM)}}$ found for the EAM α-Fe model.

The modified values of $\gamma_{\text{us(EAM)}}/\mu_{\text{slip}}b$ cited for Fe, Ni and Al are all of the order of 53% to 55% of the corresponding $\gamma_{\text{us(Frenkel)}}/\mu_{\text{slip}}b$. Thus, for

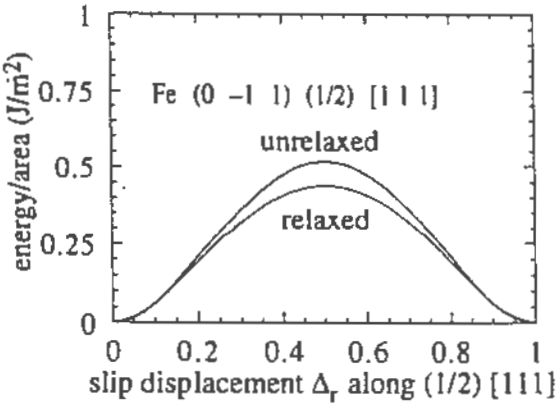

(a)

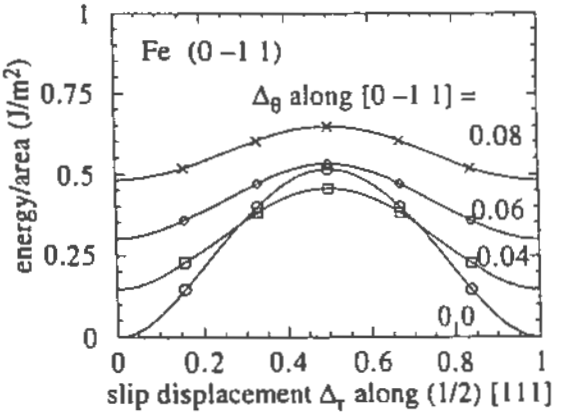

(b)

FIGURE 1.12. (a) The slip plane potential energy Ψ as function of slip displacement Δ_r along $(1/2)[111]$ on the $(0\bar{1}1)$ plane in EAM-Fe. (b) The slip plane potential energy Ψ as function of slip displacement Δ_r along $(1/2)[111]$ and opening displacement Δ_θ along $[0\bar{1}1]$ on the $(0\bar{1}1)$ plane in EAM-Fe.

later purposes (Table 1.4) in dealing with $\{111\}$ plane partial dislocations in a large class of fcc solids and with $\{110\}$ plane dislocations in a large class of bcc solids, for most of which embedded atom model results for γ_{us} are not available, the rough estimate $\gamma_{us(EAM)} = 0.54\gamma_{us(Frenkel)}$ is used in all cases. This improves upon the estimate $\gamma_{us(EAM)} = 0.7\gamma_{us(Frenkel)}$ made in a table similar to Table 1.4 by Rice (1992).

We now present results for the energy Ψ as function of block-like translational displacements $\{\Delta_r, \Delta_z, \Delta_\theta\}$, calculated based on the embedded atom method potential for α-Fe (Harrison, et al. 1990; Cheung, 1990) and Ni (Foiles and Daw, 1987). The relative positions of atoms in the two blocks are held fixed for each slip configuration. As before, Δ_r is edge-like slip, Δ_θ is opening, and Δ_z is screw-like slip. The energy surface for Δ_r displacement along $(1/2)$ $[111]$ in the $(0\bar{1}1)$ plane in α-Fe $[\Psi$ *vs.* $\Delta_r]$ is shown in Fig. 1.12(a) (also see Cheung, 1990) for $\Delta_\theta = 0$. The Ψ *vs.* Δ_r curve for relaxed conditions, along a path satisfying $\partial\Psi/\partial\Delta_\theta = 0$, is also shown, and it

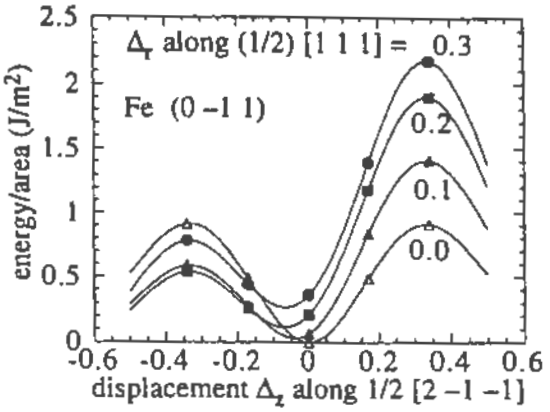

(a)

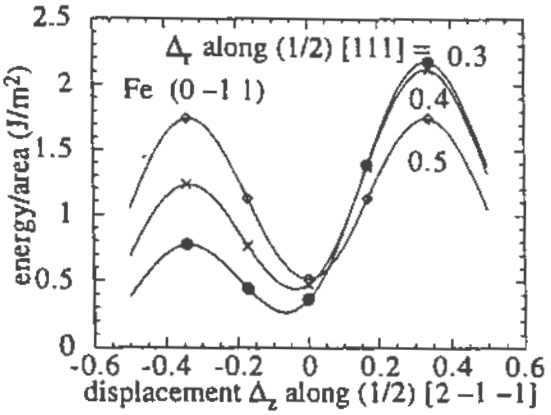

(b)

FIGURE 1.13. The potential energy Ψ as function of slip displacement Δ_r along $(1/2)[111]$ and Δ_z along $(1/2)[2\bar{1}\bar{1}]$ on the $(0\bar{1}1)$ plane in EAM-Fe. (a) shows curves for Δ_r from 0.0 to 0.3; (b) shows curves for Δ_r from 0.3 to 0.5.

has a maximum at $\gamma_{us} = 0.44 J/m^2$ as noted above. The maximum slope is $\tau_{max} = 6.41$ GPa. The energy Ψ *vs.* slip displacement Δ_r along $(1/2)\,[111]$ at various opening displacements Δ_θ along $[0\bar{1}1]$, is shown in Fig. 1.12(b). The maximum stress along the pure opening direction is $\sigma_{max} = 25.3$ GPa. The ratio $\sigma_{max}/\tau_{max} = 3.95$ for Fe.

The energy Ψ *vs.* slip displacement Δ_z along $(1/2)\,[2\bar{1}\bar{1}]$, which is perpendicular to Δ_r, for the Fe model is shown in Fig. 1.13(a) and 1.13(b), with opening Δ_θ kept at zero. The saddle-like path first deviates from the Δ_r direction (i.e., along $b = (1/2)\,[111]$) toward $(1/2)\,[\bar{2}11]$ and then gradually returns to be parallel to the Δ_r direction. Along the direction perpendicular to the saddle like path direction, the energy Ψ increases much more rapidly than along the saddle-like path direction, as seen in Figs. 1.13(a)

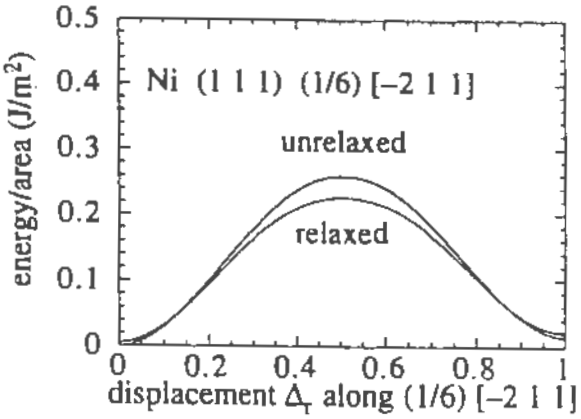

(a)

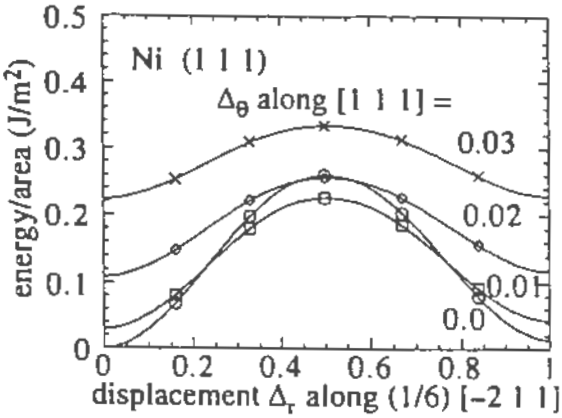

(b)

FIGURE 1.14. (a) The potential energy Ψ as function of slip displacement Δ_r along $(1/6)[\bar{2}11]$ on the (111) plane in EAM-Ni. (b) The potential energy Ψ as function of slip displacement Δ_r along $(1/6)[\bar{2}11]$ and opening displacement Δ_θ along [111] on the (111) plane in EAM-Ni.

and 1.13(b). This sort of geometry of the energy surface is, of course, the basis of the constrained path approximation discussed earlier.

The energy surface for block-like Δ_r displacement along $(1/6)$ $[\bar{2}11]$ (i.e. the partial route) in the (111) plane for the EAM model of Ni [Ψ vs. Δ_r] is shown in Fig. 1.14(a), for the unrelaxed condition when $\Delta_\theta = 0$ and the relaxed condition. The relaxed γ_{us}, is $0.226 J/m^2$. The maximum slope is $\tau_{max} = 5.54$ GPa. The energy Ψ *vs.* slip displacement Δ_r along $(1/6)$ $[\bar{2}11]$, at various opening displacements Δ_θ along [111], is shown in Fig. 1.14(b). The maximum slope along the pure opening direction is $\sigma_{max} = 28.2$ GPa. The ratio $\sigma_{max}/\tau_{max} = 5.09$ for Ni.

The energy Ψ *vs.* slip displacement Δ_z along $(1/2)$ $[0\bar{1}1]$, at various Δ_r,

TABLE 1.3. Estimates of $\gamma_{us}/\mu_{slip}b$

Solid	Frenkel Sinusoid $(b^2_{eff}/2\pi^2 bh)$	Embedded-Atom Models, Block-Like Shear	Density Functional, Homogeneous Simple Shear Strain $(W_{max}h/\mu_{slip}b)$
(1) fcc, partial dislocations, $< 211 > \{111\}$, $b = a_0/\sqrt{6}, h = a_0/\sqrt{3}, b_{eff} = b$:			
Al	0.036	0.026(u), 0.022(r),0.019($u*$)	0.042(r), 0.043(u)
Cu	0.036	—	0.042(u)
Ir	0.036	—	0.034(r), 0.043(u)
Ni	0.036	0.026(u), 0.023(r),0.020($u*$)	—
(2) bcc, $< 111 > \{110\}$, $b = \sqrt{3}a_0/2, h = a_0/\sqrt{2}, b_{eff} = b$:			
Fe	0.062	0.045(u),0.038(r),0.032($u*$)	—
(3) bcc, $< 111 > \{211\}$, $b = \sqrt{3}a_0/2, h = a_0/\sqrt{6}, b_{eff} = 2b/3$ to b :			
Cr	0.048-0.108	—	0.069(u)
Mo	0.048-0.108	—	0.056(u)
Nb	0.048-0.108	—	0.093(u)
V	0.048-0.108	—	0.100(u)
W	0.048-0.108	—	0.060(u)

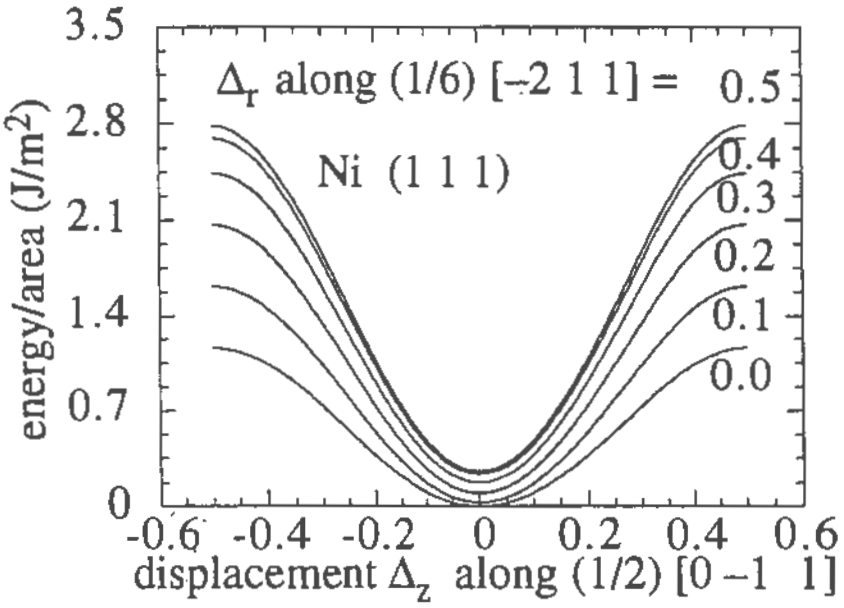

FIGURE 1.15. The potential energy Ψ as function of slip displacement Δ_r along $(1/6)[\bar{2}11]$ and Δ_z along $(1/2)[0\bar{1}1]$ on the (111) plane in EAM-Ni.

TABLE 1.4. Material Properties and γ_s/γ_{us} Ratios

Solid	$\gamma_s(T=0)$ (J/m^2)	μ_{slip} (GPa)	b (nm)	$\gamma_{us(Frenkel)}$ (J/m^2)	$\frac{\gamma_s}{\gamma_{us(Frenkel)}}$	$\frac{\gamma_s}{\gamma_{us(EAM)}}$
fcc metals:						
Ag	1.34	25.6	0.166	0.15	8.8	16.1
Al	1.20	25.1	0.165	0.15	8.1	14.6
Au	1.56	23.7	0.166	0.14	11.0	20.1
Cu	1.79	40.8	0.147	0.22	8.3	15.1
Ir	2.95†	198.	0.156	1.1	2.7	4.8
Ni	2.27	74.6	0.144	0.39	5.9	10.7
Pb	0.61	7.27	0.201	0.053	11.6	21.1
Pt	2.59	57.5	0.160	0.33	7.8	14.3
bcc metals:						
Cr	2.32	131.	0.250	2.0	1.1	2.1
Fe	2.37	69.3	0.248	1.1	2.2	4.1
K	0.13†	1.15	0.453	0.032	4.0	7.4
Li	0.53†	3.90	0.302	0.073	7.3	13.2
Mo	2.28	131.	0.273	2.2	1.0	1.9
Na	0.24†	2.43	0.366	0.055	4.4	7.9
Nb	2.57	46.9	0.286	0.83	3.1	5.6
Ta	2.90	62.8	0.286	1.1	2.6	4.7
V	2.28†	50.5	0.262	0.82	2.8	5.1
W	3.07	160.	0.274	2.7	1.1	2.1
diamond cubic:						
C	5.79†	509.	0.145	2.7	2.2	4.0
Ge	1.20†	49.2	0.231	0.41	2.9	5.4
Si	1.56†	60.5	0.195	0.42	3.7	6.7

Notes: † means γ_s is based on correlation with formation energy; Tyson (1975).

$\mu_{slip} = (c_{11} - c_{12} + c_{44})/3$.

$b = b_{partial} = a_0 < 211 > /6$ for fcc and diamond cubic; $b = a_0 < 111 > /2$ for bcc.

$\gamma_{us(Frenkel)} = 0.036\mu_{slip}b$ for fcc and diamond cubic; $\gamma_{us(Frenkel)} = 0.062\mu_{slip}b$ for bcc.

$\gamma_{us(EAM)}$ equated to $0.54\gamma_{us(Frenkel)}$ based on recent calculations of modified values, $\gamma_{us}^{(u*)}$, summarized here for EAM models of Al, Ni, and Fe. This is a change from Rice (1992) who used the estimate $\gamma_{us(EAM)} = 0.7\gamma_{us(Frenkel)}$.

for Ni is shown in Fig. 1.15, with opening Δ_θ kept at zero. The saddle-like path is strictly along the Δ_r direction. Along the direction perpendicular to the Δ_r direction, the energy Ψ increases much more rapidly than along the Δ_r direction. The constrained path approximation is thus very well justified in this case, more so than for Fe above.

Density functional theory: No directly relevant calculation for the block-like shear of one part of a metal crystal relative to another seems yet to have been reported based on quantum mechanics via density functional theory. However, such calculations appear to be feasible, as Duesbery et al. (1991) have reported energy surfaces for shear of Si along {111} planes in a manner corresponding to the introduction of an intrinsic stacking fault. The Duesbery et al. (1991) work also shows that empirical potentials, as available for Si, may agree reasonably with the quantum mechanical calculations for one direction of shear but poorly for another direction on the same crystal plane.

Paxton et al. (1991) used density functional theory in the local approximation to analyze stress-strain relations of homogeneously strained crystals, in fcc cases corresponding to simple shear parallel to {111} planes in $< 211 >$ type directions, and for bcc cases to simple shear parallel to {211} planes in $< 111 >$ type directions. These are shears leading to twinning transformations (in the softer direction of shear in each case). Paxton et al. report the maximum stress and also the maximum strain energy (say, $W_{\max}$, on a unit volume basis) encountered for simple shear in the twinning direction and in the opposite, or anti-twinning direction. The strain energy maximum, $W_{\max}$, is a rough analog of $\gamma_{\rm us}$. Both correspond to maximum energies along a shear path, but for block-like shear of one half the lattice relative to the other in the case of $\gamma_{\rm us}$ (like in Fig. 1.2, illustration d), and for homogeneous simple shear strain of the entire lattice in the case of $W_{\max}$.

Rice (1992) formed a quantity somewhat like $\gamma_{\rm us}$ from $W_{\max}$ in the following way: Since $W_{\max}$ is the maximum energy per unit volume in simple shear strain, $W_{\max}h$ is the maximum energy per unit area of slip plane associated with an interplanar separation h. This could be considered comparable to $\gamma_{\rm us}$ and thus the final column in Table 1.3 shows $W_{\max}h/\mu_{\rm slip}b$ based on $W_{\max}$ from Paxton et al. (1991) and using experimental $\mu_{\rm slip}$ values (expected to correspond within about 10% of those estimated from the density functional calculations; Paxton, private communication, 1991); $W_{\max}$ for the twinning sense is used for the fcc partial dislocation comparisons, and in the anti-twinning sense, suggested in Paxton et al. (1991), for complete {211} bcc dislocation comparisons. It is interesting that these values seem approximately compatible with the Frenkel estimates.

The experimental values for $\mu_{\rm slip}$ used in the last column of Table 1.3 (and in Table 1.4) are from Hirth and Lothe (1982) and, if not there, from Brandes (1983) or Anderson (1986). Lattice parameters a_o, used to evaluate b, are from Ashcroft and Mermin (1976).

1.10 Ductile Versus Brittle Crack Tip Response

In using the results of this paper to discuss ductile versus brittle response, in the sense of asking whether conditions for dislocation nucleation will or will not be met prior to Griffith cleavage, it is well to keep the following factors in mind.

(a) Dislocation nucleation is a process susceptible to thermal activation. The analysis given thus far here is, essentially, of temperature $T = 0$ response. The critical K's for nucleation will be reduced somewhat at finite T. The Peierls concept gives a route to treat thermally activated nucleation and some related concepts have already been uncovered in the J integral analysis of the crack tip shear (Fig. 1.4, point C) in the 2D saddle point configuration of $\delta(r)$. The fuller evaluation of the activation energy for dislocation nucleation is not yet complete, but we give some preliminary results on it later. While the K level for dislocation nucleation in some finite waiting time can, in principle, be reduced arbitrarily by increase in T (some solids may melt before there is any substantial reduction), it is interesting that the K for cleavage cannot be reduced arbitrarily and always has the Griffith level (at that T) as a lower bound. Thus increase of T should generally ease dislocation nucleation more than cleavage, and favor ductility. Our considerations in the rest of this section are for low T, when thermal activation is not an important factor.

(b) The present analysis of dislocation nucleation is approximate in many respects, and thus it will be difficult to draw definitive conclusions on ductile versus brittle response in the several borderline cases that arise. We have attained a good understanding of limits to the K^{eff} approximation, and of coupled tension-shear effects, thus far only in the isotropic case. Most importantly, perhaps, we have no very reliable estimates of γ_{us}; the $\gamma_{\text{us(Frenkel)}}$ and $\gamma_{\text{us(EAM)}}$ values of Table 1.3 may contain large errors. Also, reliable values of γ_{sf}, needed in the fcc cases, are not available for most solids.

(c) Dislocation processes not directly associated with nucleation from a crack tip may actually control brittle versus ductile response in many cases. For example, in soft solids with a high density of mobile dislocation, it may never be possible to build up enough stress at a crack tip to meet either a Griffith cleavage or a dislocation nucleation criterion, so the issue of which requires the greater local K value becomes irrelevant. Also, in solids for which dislocation mobility is low, easy nucleation of dislocations from a crack tip does not necessarily imply relaxation of stresses; cleavage may occur because such dislocations cannot move readily enough away from the crack tip so as to relax stress in its vicinity.

Accepting these limitations, consider Table 1.4. Estimates of the surface energy γ_s at $T = 0$, based on measurements that have been extrapolated to low temperature or, where noted by the cross, on correlations thus established with formation energies, are shown in the first column

based on Tyson (1975). Shear moduli $\mu_{\rm slip}$ and b are also shown (b is for a Shockley partial dislocation in the fcc and diamond cubic cases, and for a complete dislocation in the bcc cases), and the Frenkel estimate $\gamma_{\rm us(Frenkel)} = \mu_{\rm slip} b^2/2\pi^2 h$ is calculated from them, as $0.036\mu_{\rm slip}b$ for partial dislocations in fcc metals and (very uncertainly) in diamond cubic solids, and $0.062\mu_{\rm slip}b$ for complete dislocations on the {110} plane in bcc metals.

We can therefore calculate the ratios of $\gamma_s/\gamma_{\rm us}$ shown in the last two columns of Table 1.4, based respectively on $\gamma_{\rm us(Frenkel)}$ and $\gamma_{\rm us(EAM)}$, with the latter approximated as $0.54\gamma_{\rm us(Frenkel)}$ based on that being close to the modified values calculated for the three EAM models we have examined (Table 1.3) for Ni, Al, and α-Fe.

To recall now the conclusions drawn in Section 1.7, it was shown that the dislocation nucleation condition is met before that for Griffith cleavage, for the {100} cracks considered, if, under pure mode I loading, and using an isotropic elastic model, $\gamma_s/\gamma_{\rm us} > 9.1$ (fcc) or 6.3 (bcc). Those numbers were based on the $K^{\rm eff}$ approximation and were used by Rice (1992) in discussing ductile versus brittle response. We are now in a somewhat better position to estimate these limits, using corrections based on Fig. 1.8 and Table 1.2. Those corrections have been worked out only for edge dislocations, which is the appropriate case for the bcc geometry, but the second partial involved for the fcc geometry has a considerable screw component and the correction in that case is less certain. Here we provisionally use a 17% reduction in both cases, as suggested by results in Table 1.2, so that the condition for nucleation before cleavage, in the isotropic elastic case, is approximately

$$\gamma_s/\gamma_{\rm us} > 7.6({\rm fcc}) \text{ or } 5.2 \text{ (bcc)}, \tag{1.80}$$

Both required ratios were strongly reduced by small deviations from pure mode I, the fcc case most. For example, with both shear mode stress intensity factors set at 10% of $K_{\rm I}$, the requirements for dislocation nucleation to occur before Griffith cleavage, again as estimated using the $K^{\rm eff}$ approximation, dropped to $\gamma_s/\gamma_{\rm us} > 3.5$ (fcc) or 2.9 (bcc). If, provisionally, we also reduce these by the same 17% to correct for inadequacies of the $K^{\rm eff}$ approach, the limits become

$$\gamma_s/\gamma_{\rm us} > 2.9 \text{ (fcc) or } 2.4 \text{ (bcc)}. \tag{1.81}$$

(The fcc numbers in each case also depend on $\gamma_{\rm sf}/\gamma_{\rm us}$, which has been taken as 1/3 in the above inequalities; $\nu = 0.3$ is used there too.)

If we tentatively accept the $\gamma_{\rm us(EAM)}$ estimates as being close to correct, thus using the last column in Table 1.4 as estimates of $\gamma_s/\gamma_{\rm us}$, then we come to the following conclusions for the fcc metals: All the fcc metals except Ir are incapable of cleaving, even if subjected to pure mode I loading. Ir would not cleave with the 10% shear mode loading discussed, but would behave in a ductile manner. Ni is moderately near the borderline and, as an

indication that Ni may, plausibly, be thought of as a borderline material, in a brittle versus ductile sense, it is interesting to note that grain boundaries in Ni are rather easily rendered cleavable by segregation of S there and by the presence of H. If the true γ_{us} is close to the Frenkel estimate then, according to Table 1.4, both Ir and Ni would be cleavable under pure mode I, but Ni would be ductile with 10% shear mode loadings. Also, Pt, Al, and Cu are close to the borderline cleavable at low T if loaded in perfect mode I. This simplified discussion of fcc solids has assumed the same $\gamma_{us}/\mu_{slip}b$ in all material and also the same γ_{sf}/γ_{us}.

For the bcc metals, again first assume the $\gamma_{us(EAM)}$ is close to correct so that the last column of Table 1.4 gives γ_s/γ_{us}. Then the alkali metals, Li, Na and K are the standouts in terms of ductility, which is consistent with the general malleability of the alkali metals. The vanadium subgroup of the transition metals, in the order Nb, V and Ta, also stand out in Table 1.4. They fall below (marginally for Nb) the threshold for ductile crack tip response for pure mode I loading, but fit comfortably within the border for ductile response when mode I is accompanied by small loadings in the shear modes. Fe is predicted to be clearly cleavable, although it should likewise be ductilized by less than 10% shear loadings. By comparison, the chromium subgroup of transition metals, Cr, Mo and W, seem by our criterion to be irredeemably brittle, even with substantial shear mode loading.

If the Frenkel estimates of γ_{us} are, instead, somewhat closer to the mark, then the results of Table 1.4 still suggest that Li cannot be cleaved. The other alkali metals are slightly below the borderline, but are ductilized by modest shear mode loading, and Nb also would be ductilized by the 10% shear mode loading.

Diamond-cubic non-metals are also shown in Table 1.4 and γ_{us} has been extracted for them as for fcc metals, assuming that dislocations are generated by a partial route on {111} planes, and assuming (quite questionably) the same scaling of γ_{us} with $\mu_{slip}b$. All of the diamond cubic solids are predicted to be cleavable by these considerations, for pure mode I loading, although Si is somewhat susceptible to ductilization by modest shear mode loading.

The discussion concerning the emission of dissociated dislocations given in Section 1.5, which properly treats the slip energy offset by stable stacking faults and the screening effect of the emitted partial, can be used to study dislocation emission in ordered intermetallics, in which there exist dislocations with a dissociated core in pairs, which are coupled by CSF or SISF surfaces in the $L1_2$ type intermetallics; Ni_3Al is an example. Complex paths are possible for dislocation nucleation in these materials. More details may be found in Sun et. al. (1991).

Since the rough γ_{us} estimates used in Table 1.4 scale directly with $\mu_{slip}b$ for a given crystal class, the characterization of crack tip response as brittle or ductile on the basis of the size of γ_s/γ_{us} shown in that table is equivalent to characterization on the basis of $\gamma_s/\mu_{slip}b$, much as advocated by Armstrong (1966) and Rice and Thomson (1974).

TABLE 1.5. Cleavage Versus Dislocation Nucleation; Anisotropic Formulation

Solid	β	$\gamma_s/\gamma_{us(EAM)}$	$\gamma_s/(0.83\beta)\gamma_{us(EAM)}$
fcc metals [(001) cracks growing along $[\bar{1}10]$ with slip plane $(1\bar{1}1)$, for nucleation of the pair of partials (1/6) $[\bar{1}12]$ and (1/6) $[\bar{2}\bar{1}1]$]			
isotropic, $\nu = 0.3$	9.1	—	$\gamma_s/7.6\gamma_{us}$
Ag	11.1	16.1	1.74
Al	9.23	14.6	1.91
Au	11.0	20.1	2.20
Cu	11.8	15.1	1.54
Ir	10.85	4.8	0.537
Ni	12.0	10.7	1.07
Pb	10.8	21.1	2.35
Pt	9.33	14.3	1.85
bcc metals [(001) cracks growing along [010] with slip system $(1/2)[11\bar{1}](011)$]			
isotropic, $\nu = 0.3$	6.3	—	$\gamma_s/5.2\gamma_{us}$
Cr	5.83	2.1	0.432
Fe	8.77	4.1	0.559
K	14.16	7.4	0.627
Li	17.45	13.2	0.912
Mo	5.80	1.9	0.388
Na	16.33	7.9	0.584
Nb	4.88	5.6	1.38
Ta	7.34	4.7	0.777
V	5.68	5.1	1.07
W	6.38	2.1	0.395

Anisotropy considerations: We now extend the discussion to include anisotropic elastic effects. The quantity β was introduced in Eq. 1.61 and gives the bound, $\gamma_s/\gamma_{us} > \beta$, for dislocation nucleation to occur before Griffith cleavage. The expressions for β reported here are based on the K^{eff} concept. At the time of writing we have no idea of how significant the corrections, due to $\theta \neq 0$, are in the anisotropic case. We show β in Table 1.5 as it has been calculated from the elastic moduli of various fcc and bcc metals. For the fcc cases, it corresponds to nucleation of the second partial (last column of Table 1.1). A provisional guess, based on isotropic results as in Table 1.2 here, is that these may be 15% to 20% too high. We show γ_s/γ_{us}, estimated as $\gamma_s/\gamma_{us(EAM)}$ from the previous table, and show $\gamma_s/\beta\gamma_{us}$ with β provisionally replaced by 0.83 of β from the earlier columns (17% reduction, as in the isotropic case; Table 1.2). When the quantity $\gamma_s/\beta\gamma_{us}$ is greater than one, dislocation emission occurs prior to

Griffith crack extension, and when it is less than one, the opposite happens. The quantity $\gamma_s/\beta\gamma_{us}$ is tabulated in Table 1.5 for several bcc and fcc metals. The quantity β varies from 4.9 to 16.3 depending on the elastic anisotropy for bcc metals, from niobium having the lowest value to alkali metals having the highest. Therefore, the treatment of anisotropy in elasticity is important for bcc metals. In fact, it significantly changes conclusions. Nb, which was predicted to be borderline cleavable by the isotropic analysis, is now found to be ductile; Li, which was definitively ductile in the isotropic analysis is now borderline cleavable. On the other hand, β does not vary much for fcc metals, and Ir remains the standout as the cleavable fcc metal.

1.11 Extensions to Interfacial Failure

The results presented thus far may be generalized to cases where a crack lies on an interface been dissimilar materials. The case of joined isotropic solids has been worked out in detail by Beltz and Rice (1992a); a brief review of that development is given here.

Equations 1.72 may be generalized by making use of the interfacial crack tip field, in which stresses are given by

$$\sigma_{\alpha\beta} = \frac{1}{\sqrt{2\pi r}}\left[\mathrm{Re}(Kr^{i\epsilon})\Sigma^{\mathrm{I}}_{\alpha\beta}(\theta) + \mathrm{Im}(Kr^{i\epsilon})\Sigma^{\mathrm{II}}_{\alpha\beta}(\theta) + K_{\mathrm{III}}\Sigma^{\mathrm{III}}_{\alpha\beta}(\theta)\right] \quad (\alpha,\beta = r,\theta,z) \tag{1.82}$$

Only in-plane loadings are considered here. The functions $\Sigma_{\alpha\beta}(\theta)$ correspond to tractions across the interface at $\theta = 0$ of tensile, in-plane, and anti-plane shear type, so that

$$(\sigma_{\theta\theta} + i\sigma_{r\theta})_{\theta=0} = \frac{Kr^{i\epsilon}}{\sqrt{2\pi r}},\ (\sigma_{z\theta})_{\theta=0} = \frac{K_{\mathrm{III}}}{\sqrt{2\pi r}}. \tag{1.83}$$

K is the complex stress intensity factor which characterizes the inherently coupled in-plane modes. The parameter ϵ is given by

$$\epsilon = \frac{1}{2\pi}\ln\left[\frac{(3-4\nu_1)/\mu_1 + 1/\mu_2}{1/\mu_1 + (3-4\nu_2)/\mu_2}\right] \tag{1.84}$$

where μ and ν refer to the shear modulus and Poisson's ratio, respectively. Subscript 1 refers to the material on top, occupying $0 < \theta < \pi$, which is taken to be a metal (i.e., can sustain a dislocation-like process), and subscript 2 refers to a ceramic phase (i.e., no dislocation activity is assumed to occur). We have $\Sigma^{\mathrm{I}}_{\theta\theta}(0) = \Sigma^{\mathrm{II}}_{r\theta}(0) = 1$ and the full functions $\Sigma_{\alpha\beta}(\theta)$ are given by Rice, Suo, and Wang (1990) and can be extracted from discussions of the bimaterial elastic singular field (e.g., Rice (1988)).

The generalization of Eqs. 1.77 may now be written as

$$\begin{aligned}
&\tau\left(\Delta_r(r), \Delta_\theta(r)\right) \\
&\quad = \frac{1}{\sqrt{2\pi r}} \left\{ \mathrm{Re}\left[\mathrm{Kr}^{i\varepsilon}\right] \Sigma^{\mathrm{I}}_{r\theta}(\theta;\varepsilon) + \mathrm{Im}\left[\mathrm{Kr}^{i\varepsilon}\right] \Sigma^{\mathrm{II}}_{r\theta}(\theta;\varepsilon) \right\} \\
&\quad - \frac{\mu_1}{2\pi(1-\nu_1)} \int_0^\infty g_{11}(r,\rho;\theta,\varepsilon) \frac{\partial \delta_r(\rho)}{\partial \rho} d\rho \\
&\quad - \frac{\mu_1}{2\pi(1-\nu_1)} \int_0^\infty g_{12}(r,\rho;\theta,\varepsilon) \frac{\partial \delta_\theta(\rho)}{\partial \rho} d\rho
\end{aligned} \tag{1.85a}$$

$$\begin{aligned}
&\sigma\left(\Delta_r(r), \Delta_\theta(r)\right) \\
&\quad = \frac{1}{\sqrt{2\pi r}} \left\{ \mathrm{Re}\left[\mathrm{Kr}^{i\varepsilon}\right] \Sigma^{\mathrm{I}}_{\theta\theta}(\theta;\varepsilon) + \mathrm{Im}\left[\mathrm{Kr}^{i\varepsilon}\right] \Sigma^{\mathrm{II}}_{\theta\theta}(\theta;\varepsilon) \right\} \\
&\quad - \frac{\mu_1}{2\pi(1-\nu_1)} \int_0^\infty g_{21}(r,\rho;\theta,\varepsilon) \frac{\partial \delta_r(\rho)}{\partial \rho} d\rho \\
&\quad - \frac{\mu_1}{2\pi(1-\nu_1)} \int_0^\infty g_{22}(r,\rho;\theta,\varepsilon) \frac{\partial \delta_\theta(\rho)}{\partial \rho} d\rho
\end{aligned} \tag{1.85b}$$

The kernel functions g_{11}, g_{12}, g_{21}, and g_{22} are taken from the elasticity solution for a Volterra dislocation in the presence of an interfacial crack, and may be found in complex form (Suo, 1989).

Solutions to the pair of integral Eqs. 1.85 have been found using physical constants appropriate for copper bonded to sapphire (Beltz and Rice, 1992a) and iron bonded to titanium carbide (Beltz, 1991). As discussed by Rice, Suo, and Wang (1990), $r^{i\varepsilon}$ can be replaced by $b^{i\varepsilon}$, and the analysis is tenable when $Kb^{i\varepsilon}$ has a positive real part.

1.12 Experimental Observations

The actual observation of dislocation emission from crack tips has been achieved by the use of several experimental techniques. In work by Burns (1986), etch pit techniques were employed to observe edge dislocations on slip planes which emanated from a crack which had been cut parallel to the {110} planes in lithium fluoride. X-ray topography has been used by Michot and George (1986) to carry out similar observations in silicon. Possibly the most notable observations of dislocation emission is the T.E.M. work of Ohr (1985, 1986), which has the advantage that emission could be observed in-situ in several materials, including fcc and bcc metals with a high resolution. In these experiments, the critical applied stress intensity factor K_e to emit a dislocation was indirectly measured; they were in moderate agreement for several metals with the theoretical values of K_e as predicted by the Rice-Thomson model. More recently, Chiao and Clarke (1989) directly observed

emitting dislocations in silicon and claimed reasonable agreement of the inferred K_e with Rice-Thomson modeling.

The first experimental evidence that the macroscopic behavior of an interface could be rationalized based on the competition between dislocation emission and cleavage was given by Wang and Anderson (1990), in their work on symmetric tilt bicrystals of copper. In this work, a directional effect on the toughness of the grain boundary in a Σ 9[110](2$\bar{2}$1) bicrystal was observed, in which two specimens were cut and notched along the boundary such that a crack would run in the opposite directions [$\bar{1}$14] and [1$\bar{1}\bar{4}$], respectively. The specimens were fatigued under a cyclic mode I loading of increasing amplitude. The specimen with the [1$\bar{1}\bar{4}$] cracking direction broke along the interface when the maximum normal stress reached $\sigma = 28.1$MPa, corresponding to $G \approx 28 J/m^2$. An intergranular fracture surface with cleavage "tongues" was observed. The other specimen, with a cracking direction of [$\bar{1}$14], was loaded under identical conditions and eventually fractured at a normal stress of 76.7 MPa. The fracture surface contained large regions of ductile transgranular fracture and plastic tearing, and the G value, $> 210 J/m^2$, was beyond the reliably measurable range for elastic fracture mechanics. The only difference between these two specimens was the cracking direction, hence it was concluded that the difference in ease with which dislocations could be nucleated at each crack tip was the cause of this behavior, as predicted nucleation loads are quite different for the two growth directions. Further, continuum plasticity analyses by Saeedvafa (1991) and Mohan et. al. (1991), suggested very little difference in the stress state ahead of the crack tip, for the two growth directions, and do not suggest a more macroscopic explanation of the experiments.

Most recently, Beltz and Wang (1992) have performed experiments on copper crystals bonded on the same {221} copper face to sapphire, to form a layered beam subjected to four-point bending (see Fig. 1.16). Again, a directional dependence of toughness was observed. In their experiment, the ductile direction was observed to be [1$\bar{1}\bar{4}$], the *opposite* of the ductile direction with the Wang-Anderson bicrystal specimen. This result was predicted by theory, however, and is elaborated on in Beltz and Rice (1992a) in terms of the Peierls-type nucleation model; it follows from different mode I/II mixture in the two specimens.

1.13 The Activation Energy for Dislocation Nucleation

Thus far, the analysis of dislocation nucleation rigorously holds true at zero Kelvin; i.e., thermal effects are neglected, except possibly through the weak temperature dependence of the elastic constants that enter the analysis. As discussed earlier in connection with Fig. 1.4, a saddle-point configuration

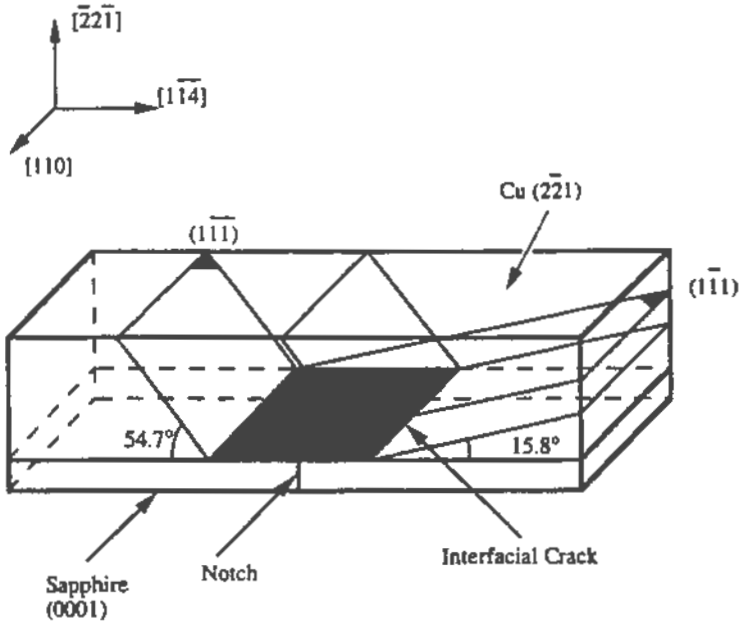

FIGURE 1.16. Diagram of specimen tested by Beltz and Wang (1992): a copper single crystal with {221} face bonded to sapphire; loaded in bending with crack tips along [110].

TABLE 1.6. Activation Energies

$\frac{G}{G_{crit}}$	$\frac{(1-\nu)\Delta_{act}}{\mu b^2}$	$\frac{\Delta E_{Cu,partial}}{kT_{room}}$	$\frac{\Delta E_{Fe,fulldisl.}}{kT_{room}}$
0.2	1.25×10^{-1}	29.4	239.6
0.3	9.05×10^{-2}	21.3	173.5
0.4	6.55×10^{-2}	15.4	125.5
0.5	4.62×10^{-2}	10.09	88.6
0.6	3.10×10^{-2}	7.29	59.4
0.7	1.90×10^{-2}	4.47	36.4
0.8	9.85×10^{-3}	2.31	18.9
0.9	3.32×10^{-3}	0.780	6.36
1.0	0	0	0

exists with 2D form corresponding to point C. The total energy corresponding to the system at C less the total energy at A would correspond to an activation energy; this energy could be thought of as the amount of energy due to thermal vibrations necessary to emit an incipient dislocation which is initially loaded below $G_{\rm crit}$. A two-dimensional simplification to the problem reduces to that of finding a *second* solution to Eq. 1.55, for a given applied load. To be realistic, the activation process would take place over a localized region, i.e. in the form of a dislocation loop that jumps out. At the time of writing, we have analyzed such solutions only for the case $\theta = 0$, $\phi = 0$, and using the Frenkel form of $\tau = f(\delta)$ and explicitly considering slip only, like in Sections 1.2 to 1.4 of the paper. In that case Eq. 1.55 corresponds to rendering stationary the energy functional (Rice, 1992)

$$U[\delta(r)] = U_0 + \int_0^\infty \Phi(\delta(r))dr + \int_0^\infty \frac{1}{2} s[\delta(r)]\delta(r)dr - \int_0^\infty \frac{K_{\rm II}}{\sqrt{2\pi r}}\delta(r)dr \tag{1.86}$$

with

$$s[\delta(r)] = \frac{\mu}{2\pi(1-\nu)} \int_0^\infty \sqrt{\frac{\rho}{r}} \frac{d\delta(\rho)/d\rho}{r-\rho} d\rho \tag{1.87}$$

Here $U[\delta(r)]$ is the energy of a slipped configuration per unit distance along the crack front. Thus, for $G < G_{\rm crit}$ ($= \gamma_{\rm us}$ in this case) and with $\delta_{\rm min}(r)$ and $\delta_{\rm sad}(r)$ representing $\delta(r)$ for the energy minimum and saddle-point solutions (with values of $\delta(0)$ corresponding respectively to points A and C in Fig. 1.4), we can calculate a 2D activation energy

$$\Delta U_{\rm act} = U[\delta_{\rm sad}(r)] - U[\delta_{\rm min}(r)] \tag{1.88}$$

Results are shown in Table 1.6. Also, we show by the dashed line in Fig. 1.11 the slip function $\delta_{\rm sad}(r)$ corresponding to $G = 0.9G_{\rm crit}$, a case for which $\delta_{\rm min}(r)$ is also shown.

The actual activation process is inherently three-dimensional, at least as regards the saddle point configuration. An asymptotic analysis is underway of this 3D phenomenon by Beltz and Rice (1992b). A very rough approximation to their result for the activation energy ΔE involves multiplying the two-dimensional activation energy $\Delta U_{\rm act}$ (an energy per unit dislocation length) by about five atomic spacings, which is a plausible length scale for the activation process.

Table 1.6 shows the results (from the two-dimensional analysis, assuming an activated dislocation length of 5b, $\Delta E \approx 5b\Delta U_{\rm act}$) for a partial dislocation in copper and a full dislocation in iron, with a coplanar slip plane and a mode II loading. The ΔE estimates are listed in units of kT as evaluated at room temperature. An elementary calculation of a "cutoff" $\Delta E/kT$ for

spontaneous nucleation is discussed by Beltz and Rice (1992b) and uses the formula

$$\upsilon = n(c_{\text{shear}}/b)\exp(-\Delta E/kT) \tag{1.89}$$

where υ is interpreted as the frequency of spontaneous nucleation events, n is taken as the number of nucleation sites in a typical span of crack front, taken here as 1 mm (i.e., $n = 1\text{mm}/5b$) and c_{shear} is the transverse shear wave speed, so that c_{shear}/b is an approximate attempt frequency. Here, c_{shear} is taken as 3 km/sec. Assuming that $\upsilon \approx 10^6$/sec describes spontaneous nucleation on a laboratory time scale, solution of Eq. 1.89 gives a borderline of $\Delta E/kT \approx 25$. Examination of Table 1.6 leads to the conclusion that thermal activation would be sufficient (at room temperature) to spontaneously emit a partial dislocation in copper at loadings of $G \approx (0.2-0.3)G_{\text{crit}}$ or greater, and a full dislocation in iron at loadings of $G \approx (0.7-0.8)G_{\text{crit}}$ or greater, where G_{crit} is the critical loading for dislocation nucleation without help from thermal activation. At $T = 2T_{\text{room}}$, these values for spontaneous nucleation would, e.g., change to approximately $0.1G_{\text{crit}}$ for Cu and $0.6G_{\text{crit}}$ for Fe.

1.14 Summary and Conclusions

A new analysis of dislocation nucleation from a crack tip is outlined based on the Peierls concept as applied to a slip plane emanating from the tip. An exact solution for the nucleation criterion is found using the J integral when the crack and slip plane coincide, at least within simplifying assumptions that consider only shear sliding between lattice planes, in forming a dislocation. The exact solution is also extended to the nucleation of dissociated dislocations, with complete results found for the nucleation of a pair of Shockley partials in fcc solids. For cases of greater interest, in which the slip and crack planes do not coincide ($\theta \neq 0$) but, rather, intersect along the crack tip, an approximate solutions for the nucleation criterion are given based on effective shear stress intensity factors along the slip plane, and exact solutions from numerical solution of appropriate integral equations are also discussed, including those which take fully into account the coupling between tension and shear across the slip plane.

The core width of the incipient dislocation at the threshold of instability is estimated to be about 3 times the corresponding width for an isolated dislocation in an otherwise perfect lattice, so that conditions seem favorable to use of the Peierls concept. Further, while previous treatments of nucleation have generally been based on elasticity solutions for fully formed dislocations located very near the crack tip, this analysis shows that maximum shear slippage at the tip is, at the moment of instability, only of the order of half that for a fully formed dislocation.

The results highlight a new solid state parameter γ_{us}, called the unstable stacking energy, which measures the resistance to dislocation nucleation at a crack tip. Critical stress intensity factors at nucleation scale with $\sqrt{\gamma_{us}}$. Here γ_{us} is the maximum energy, per unit area, encountered in the block-like shear of one half of a crystal relative to the other, along a slip plane in the direction of shear which forms a lattice dislocation. Also, some features of the 2D activated configuration (energy saddle point) have been derived for a crack tip loaded below the level for instantaneous nucleation.

There are, at present, only quite uncertain estimates of γ_{us}. The sheared atomic lattice geometry to which it corresponds is however, a relatively simple one, periodic in the two directions along the slip plane and involving simple block-like translation of atoms above and below. Thus, it is to be hoped that the parameter may be susceptible to quantum electronic calculation, and such work is encouraged (the same for stacking fault and anti-phase boundary energy terms, which also enter the nucleation criteria for dissociated dislocations).

Allowing for considerable uncertainties in γ_{us}, the evaluation of the competition over whether the condition for Griffith cleavage, or for dislocation generation and blunting, is met first at a crack tip leads to results that seem generally consistent with known brittle versus ductile response of fcc and bcc metals. The results also suggest that the outcome of this competition is often extremely sensitive to small amounts of mode II and mode III shear loading superposed on a basic mode I tensile loading; the shear loadings promote ductile response.

The new analysis of dislocation nucleation given here, like that formulated by Rice and Thomson (1974), is developed only for cases in which the crack tip lies in a slip plane. It has been noted (Argon, 1987; Dragone and Nix, 1988) that the maximally stressed slip plane is sometimes one which intersects the crack tip at a single point but does not contain it. There seems to be no simple way of extending the present approach to such cases.

Added Note: Our analysis of partial dislocation emission in §1.5 and §1.6 is incorrect in the following sense. As A.S. Argon and J. F. Knott indicated to us, the atomic geometry of the fcc slip plane forces partials to nucleate in an *ordered sequence*, not competitively. Our equations are correct if used first to evaluate the loads for nucleation of partial A (as in Eq. (1.26)) and then to evaluate the load for partial B (as in Eqs. (1.20) and (1.32)). For the crack geometry considered in §1.6 and §1.10, the proper sequence is first a partial with $\phi = \pm 60°$, and then the partial with $\phi = 0°$. Consequently, Eq. (1.67) should become $\gamma_s/\gamma_{us} > 11.8$, for emission before cleavage under mode I, and $\gamma_s/\gamma_{us} > 5.3$ under mode I plus 10% shear modes. The stacking fault energy γ_{sf} does not affect the nucleation of the first partial at $\theta = \pm 60°$ and the second, at $\phi = 0°$, follows spontaneously for the near-mode I conditions assumed. With the ~17% correction to the K^{eff} concept, the conditions for dislocation nucleation before cleavage in §1.10 change as

follows: For a mode I load Eq. (1.80) should read $\gamma_s/\gamma_{us} > 9.8$ (fcc) or 5.2 (bcc), and for mode I plus 10% shear modes Eq. (1.81) should read $\gamma_s/\gamma_{us} > 4.4$ (fcc) or 2.4 (bcc). These corrections do not affect our conclusions on brittle vs. ductile response for the fcc metals.

We are pleased to dedicate the paper to Professor Frank A. McClintock.

Acknowledgments: The group of studies reported here has been supported primarily by the Office of Naval Research, Mechanics Division (grant N00014-90-J-1379), and also by the National Science Foundation Materials Research Laboratory at Harvard (grant DMR-89-20490), and a University Research Initiative (subcontract P0AVB38639-0 from the University of California, Santa Barbara, based on ONR/DARPA contract N00014-86-K-0753). Some of the computations were carried out under NSF support at the Pittsburgh Supercomputing Center.

REFERENCES

Anderson, P. M. (1986). Ductile and brittle crack tip response, Ph.D. Thesis, Div. of Applied Sciences, Harvard University, Cambridge, MA, USA.

Argon, A. S. (1987). Brittle to ductile transition in cleavage fracture, Acta Met., 35:185–196.

Armstrong, R. W. (1966). Cleavage crack propagation within crystals by the Griffith mechanism versus a dislocation mechanism, Mater. Sci. Eng., 1:251–256.

Ashcroft, N. W. and Mermin, N. D. (1976). Solid State Physics, Holt, Rinehart and Winston, New York.

Barnett, D. and Asaro, R. J. (1972). The fracture mechanics of slit-like cracks in anisotropic elastic media, J. Mech. Phys. Solids, 20: 353–366.

Beltz, G. E. (1991). Unpublished research, on the emission of dislocations on inclined slip planes in the Fe/TiC system.

Beltz, G. E. and Rice, J. R. (1991). Dislocation nucleation versus cleavage decohesion at crack tips, In Lowe, T. C., Rollett, A. D., Follansbee, P. S. and Daehn, G. S., editors, *Modeling the Deformation of Crystalline Solids*, TMS, pages 457–480.

Beltz, G. E., and Rice, J. R. (1992a). Dislocation nucleation at metal/ceramic interfaces, Acta Met., in press.

Beltz, G.E., and Rice, J. R. (1992b). Research in progress, on the 2D and 3D calculations of the activation energy for dislocation nucleation.

Beltz, G. E., and Wang, J.-S. (1992). Crack direction effects along copper/sapphire interfaces, Acta Met., in press.

Brandes, E. A. (1983). *Smithells Metals Reference Book*, 6th ed., Butterworths, London.

Burns, S. J. (1986). Crack tip dislocation nucleation observations in bulk specimens, Scripta Met., 20:1489–1494.

Cheung, K. (1990). Atomistic study of dislocation nucleation at a crack tip, Ph.D. Thesis, Dept. of Nuclear Engineering, MIT, Cambridge, MA, USA.

Cheung, K., Yip, S. and Argon, A. S. (1991). Activation analysis of dislocation nucleation from a crack tip in α-Fe, J. Appl. Phys., 69:2088–2096.

Chiao, Y.-H., and Clarke, D. R. (1989). Direct observation of dislocation emission from crack tips in silicon at high temperatures, Acta Met., 37:203–219.

Daw, M. S., and Baskes, M. I. (1984). Embedded-atom method: Derivation and application to impurities and other defects in metals, Phys. Rev. B, 29:6443–6453.

Dragone, T. L., and Nix, W. D. (1988). Crack tip stress fields and dislocation nucleation in anisotropic materials, Scripta Met., 22:431–435.

Duesbery, M. S., Michel, D. J., Kaxiras, E. and Joos, B. (1991). Molecular dynamics studies of defects in Si, In Bristowe, P. D., Epperson, J. E., Griffith, J. E. and Liliental-Weber, Z., editors, *Defects in Materials*, Materials Research Society, 209:125–130.

Eshelby, J. D. (1970). Energy relations and the energy-momentum tensor in continuum mechanics, In Kanninen, M. F., Adler, W. F., Rosenfield, A. R. and Jaffee, R. I., editors, *Inelastic Behavior of Solids*, McGraw-Hill, New York, pages 77–115.

Foiles, S. M., Baskes, M. I. and Daw, M. S. (1986). Embedded-atom-method functions for the fcc metals Cu, Ag, Au, Ni, Pd, Pt, and their alloys, Phys. Rev. B., 33:7983–7991.

Foiles, S. M., and Daw, M. S. (1987). Application of the embedded atom method to Ni^3Al, J. Mater. Res., 2:5–15.

Harrison, R. J., Spaepen, F., Voter, A. F. and Chen, A. F. (1990). Structure of grain boundaries in iron, In Olson, G. B., Azrin, M. and Wright, E. S., editors, *Innovations in Ultrahigh-Strength Steel Technology*, Plenum Press, pages 651–675.

Hirth, J. P., and Lothe, J. (1982). *Theory of Dislocations*, 2nd Edition, McGraw Hill, New York.

Hoagland, R. G., Daw, M. S., Foiles, S. M. and Baskes, M. I. (1990). An atomic model of crack tip deformation in aluminum using an embedded atom potential, J. Mater. Res., 5:313–324.

Kelly, A., Tyson, W. R. and Cottrell, A. H. (1967). Ductile and brittle crystals, Phil. Mag. 15, pages 567–586.

Lin, I.-H., and Thomson, R. (1986). Cleavage, dislocation emission, and shielding for cracks under general loading, Acta Met., 34:187–206.

Michot, G., and George, A. (1986). Dislocation emission from cracks — observations by x-ray topography in silicon, Scripta Met., 20:1495–1500.

Mohan, R., Ortiz, M and Shih, C. F. (1991). Crack-tip fields in ductile single crystals and bicrystals, In Lowe, T. C., Rollett, A. D., Follansbee, P. S. and Daehn, G. S., editors, *Modeling the Deformation of Crystalline Solids*, TMS, pages 481–498.

Nabarro, F. R. N. (1947). Dislocations in a simple cubic lattice, Proc. Phys. Soc., 59:256–272.

Ohr, S. M. (1985). An electron microscope study of crack tip deformation and its impact on the dislocation theory of fracture, Mat. Sci. and Engr., 72:1–35.

Ohr, S. M. (1986). Electron microscope studies of dislocation emission from cracks, Scripta Metall., 20:1501–1506.

Paxton, A. T., Gumbsch, P. and Methfessel, M. (1991). A quantum mechanical calculation of the theoretical strength of metals, Phil. Mag. Lett., 63:267–274.

Peierls, R. E. (1940). The size of a dislocation, Proc. Phys. Soc., 52:34–37.

Rice, J. R. (1968a). A path independent integral and the approximate analysis of strain concentration by notches and cracks, J. Appl. Mech., 35:379–386.

Rice, J. R. (1968b). Mathematical analysis in the mechanics of fracture, Ch. 3 of Liebowitz, H., editor, *Fracture: An Advanced Treatise* (vol. 2, *Mathematical Fundamentals*), Academic Press, NY, pages 191–311.

Rice, J. R. (1985). Conserved integrals and energetic forces, In Bilby, B. A., Miller, K. J. and Willis, J. R., *Fundamentals of Deformation and Fracture* (Eshelby Memorial Symposium), Cambridge University Press, pages 33–56.

Rice, J. R. (1987). Mechanics of brittle cracking of crystal lattices and interfaces, In Latanision, R. M. and Jones, R. H., editors, *Chemistry and Physics of Fracture*, Martinus Nijhoff Publishers, Dordrecht, pages 23–43.

Rice, J. R. (1988). Elastic fracture mechanics concepts for interfacial cracks, In J. Appl. Mech., 55:98–103.

Rice, J. R. (1992). Dislocation nucleation from a crack tip: an analysis based on the Peierls concept, to be published in J. Mech. Phys. Solids, 40:239–271.

Rice, J. R., Suo, Z. and Wang, J.-S. (1990). Mechanics and thermodynamics of brittle interfacial failure in bimaterial systems, In Rühle, M., Evans, A. G., Ashby, M. F. and Hirth, J. P., editors, *Metal-Ceramic Interfaces*, Pergamon Press, Oxford, pages 269–294.

Rice, J. R., and Thomson, R. M. (1974). Ductile *vs.* brittle behavior of crystals, Phil. Mag., 29:73–97.

Rice, J. R., and Wang, J.-S. (1989). Embrittlement of interfaces by solute segregation, Mat. Sci. and Engr., A107:23–40.

Saeedvafa, M. (1991). Orientation dependence of fracture in copper bicrystals with symmetric tilt boundaries, submitted to Mech. Mat.

Schoeck, G. (1991). Dislocation emission from crack tips, Phil. Mag., 63:111–120.

Stroh, A. H. (1958). Dislocations and cracks in anisotropic elasticity, Phil. Mag. 3:625–646.

Suo, Z. (1989). Mechanics of interface fracture, Ph.D. Thesis, Div. of Applied Sciences, Harvard University, Cambridge, MA, USA.

Sun, Y. (1991). Unpublished work, on EAM fits for α-Fe, Al, and Ni.

Sun, Y., Beltz, G. E. and Rice, J. R. (1992). Research in progress, on embedded atom models as a basis for estimating normal stress effects in dislocation nucleation.

Sun, Y., and Rice, J. R. (1992). Research in progress, on the anisotropic elastic formulation of dislocation nucleation.

Sun, Y., Rice, J. R. and Truskinovsky, L. (1991). Dislocation nucleation versus cleavage in Ni_3Al and Ni, In Johnson, L. A., Pope, D. T. and Stiegler, J. O., editors, *High-Temperature Ordered Intermetallic Alloys*, Materials Research Society, 213:243–248.

Tyson, W. R. (1975). Surface energies of solid metals, Canadian Metallurgical Quarterly, 14:307–314.

Vitek, V. (1968). Intrinsic stacking faults in body-centered cubic crystals, Phil. Mag., 18:773–786.

Vitek, V., Lejcek, L. and Bowen, D. K. (1972). On the factors controlling the structure of dislocation cores in bcc crystals, In Gehlen, P. C., Beeler, J. R. and Jaffee, R. I., editors, *Interatomic Potentials and Simulation of Lattice Defects*, Plenum Press, New York, pages 493–508.

Wang, J.-S., and Anderson, P. M. (1991). Fracture behavior of embrittled fcc metal bicrystals and its misorientation dependence, Acta Met., 39:779–789.

Weertman, J. (1981). Crack tip blunting by dislocation pair creation and separation, Phil. Mag., 43:1103–1123.

Willis, J. R. (1967). A comparison of the fracture criteria of Griffith and Barenblatt, J. Mech. Phys. of Solids, 15:151–162.

Yamaguchi, M., Vitek, V. and Pope, D. (1981). Planar faults in the $L1_2$ lattice, stability and structure, Phil. Mag., 43, 1027-1044.